CHALMERS
UNIVERSITY OF TECHNOLOGY

Electrified District Heating Plants using Thermochemical Energy Storage

Economic assessment of the implementation of an iron redox solids cycle in fluidized-bed-based district heating plants

Master's thesis within the Erasmus+ Programme

JAVIER CORTÉS ROMEA

Department of Space, Earth and Environment
Division of Energy Technology
Chalmers University of Technology
Gothenburg, Sweden 2023

Master's thesis 2023

Electrified District Heating Plants using Thermochemical Energy Storage

Economic assessment of the implementation of an iron redox solids cycle in fluidized-bed-based district heating plants

JAVIER CORTÉS ROMEA

CHALMERS
UNIVERSITY OF TECHNOLOGY

Department of Space, Earth and Environment
Division of Energy Technology
Fluidization Research Group
Chalmers University of Technology
Gothenburg, Sweden 2023

Electrified District Heating Plants using Thermochemical Energy Storage
Economic assessment of the implementation of an iron redox solids cycle in fluidized-bed-based district heating plants
JAVIER CORTÉS ROMEA

© JAVIER CORTÉS ROMEA, 2023.

Supervisor: Guillermo Martínez, Department of Space, Earth and Environment
Co-supervisor: Alla Toktarova, Department of Space, Earth and Environment
Co-supervisor: Diana Carolina Guío-Perez, Department of Space, Earth and Environment
Examiner: David Pallarès, Department of Space, Earth and Environment

Master's Thesis 2023
Department of Space, Earth and Environment
Division of Energy Technology
Fluidization Research Group
Chalmers University of Technology
SE-412 96 Gothenburg
Telephone +46 31 772 1000

Cover: Feskekörka is an indoor fish market in Gothenburg, Sweden.

Typeset in LaTeX
Printed by Chalmers Reproservice
Gothenburg, Sweden 2023

Electrified District Heating Plants using Thermochemical Energy Storage
Economic assessment of the implementation of an iron redox solids cycle in fluidized-bed-based district heating plants
JAVIER CORTÉS ROMEA
Department of Space, Earth and Environment
Chalmers University of Technology

Abstract

Carbon emissions, particularly from electricity and heat generation, remain a major cause of global warming, accounting for 40 % of global CO_2 emissions in 2021. To decarbonize the electricity sector, the use of variable renewable energy (VRE) sources is being encouraged. At the same time, variation management strategies are required to maximize the value of VRE as its share increases and to reduce curtailing. Meanwhile, the heating sector is called to transit into an electrified scheme, which should also reduce the use of biomass, as it is becoming a limited resource. Thermochemical energy storage (TCES) systems, particularly high-temperature solid cycles, such as metal redox-looping, provide a solution for both the electricity and heating sectors. TCES systems have the potential to use non-dispatchable renewable electricity to reduce a metal oxide, which can be stored for long periods of time at ambient conditions and subsequently oxidized to release the stored energy in the form of high-temperature heat (700-1100 °C).

This thesis presents an economic assessment of the retrofitting of biomass-firing DH plants by incorporating a TCES scheme based on metal-oxide redox cycles. The viability of the proposed system is analyzed through a case study. Sweden was selected for the study case owing to the existence of a metal extraction and processing infrastructure and the availability of DH plants based on fluidized bed (FB) boilers. The cost of the retrofit was estimated and used as an input in a linear cost optimization model to investigate the impact of the electricity price variability on the cost-optimal size and operation of an electrified DH plant. Today's typical capacity of biomass-firing DH plants was selected as a reference. The results of the study indicate that as a consequence of including storage the operation of the plant can be adapted to respond to electricity price variations. The proposed process can cover the heat demand at a cost of 55-70 €/MWh. The proposed main scheme proved profitable for the investigated scenarios of electricity price variation, while the economic viability of using solid oxide electrolyzer cells (SOEC) instead of alkaline ones or adding hydrogen storage depends on the potential cost reductions in these technologies in the future.

Keywords: variable renewable energy (VRE), thermochemical energy storage (TCES), iron looping, district heating (DH), electricity system, Sweden, decarbonization, electrification.

Acknowledgements

First of all, I would like to thank my supervisors, Guillermo Martínez Castilla, Alla Toktarova and Carolina Guío-Pérez, for their support, guidance and help throughout these months. I feel very fortunate to have been able to work with you and learn from the best. Guillermo, thank you for always having your door open day after day to discuss cost equations or ideas for improving my work. I really appreciate how you have guided me all along this path. Thank you, Alla, for your support and patience when the simulations did not come out in the way we wished. I have learned a lot from you and your contagious positivity. Carolina, thank you for your great help in my research and for always looking for time to give me very valuable feedback. It's been an honor to learn from someone like you.

Thanks to David Pallarès, my examiner, for welcoming me into the fluidization group and for making Catalonia not so far from Göteborg. Thanks also to all employees of the Energy Technology division for making this workplace a pleasant and warm environment. Thanks to my fellow masters thesis students, William, Ulla and Max. I wish you the best in the future.

This would not have been possible without my friends. Thank you, Aleix, for embarking with me on this journey and coming to Göteborg, it has been a great adventure. Special thanks also to the friends I made in this city, you are all part of this unique experience.

Laura, thank you for always being by my side and encouraging me to keep going. It is a joy to continue building together. Finally, thanks to my parents Jose Manuel and Sole, and my sister Marta, for their unconditional love and support in everything I do.

Javier Cortés Romea, Göteborg, February 2023

List of Acronyms

AEC	alkaline electrolysis cell
BEC	bare-erected cost
BF	blast furnace
BUA	bottom-up approach
CaL	carbonate looping
CAPEX	capital expenditure
CHP	combined heat and power
DH	district heating
DRI	direct reduced iron
EAF	electric arc furnace
EC	European Commission
EU	European Union
FB	fluidized bed
GAMS	general algebraic modelling system
H2D	Hours-to-Decades
HBI	hot briquetted iron
HP	heat pump
IRR	internal rate of return
NPV	net present value
PBP	payback period
PEM	polymer electrolyte membrane
SOEC	solid oxide electrolysis cell
SS-HX	solid-solid heat exchanger
TCES	thermochemical energy storage
TPC	total plant cost
VRE	variable renewable energy

Nomenclature

C	cost
C_p^{inv}	investment cost of technology p
$C_p^{O\&M,fix}$	fixed operating and maintenance cost of technology p
$C_{p,t}^{run}$	running cost of technology p in time-step t
C^{tot}	total heat production cost
C_0	reference cost
řC	degrees Celsius
CF_0	initial investment
CF_n	net cash-flow during a single period n
D_t^{heat}	heat demand at time-step t
e_p	efficiency of storage technology p
f	scale factor
$g_{p,t}$	generation of heat and production of commodities of technology p at time-step t
i_p	capacity investment of in technology p
N	number of time periods
n	time period
p	index of technologies
P	set of all technologies
P^{hpr}	subset of P that includes all heat production technologies (electrolyzer, reduction reactor, oxidation reactor)
P^{str}	subset of P that includes all storage technologies (hydrogen storage, reduced iron storage, iron oxide storage)
r	discount rate
S_0	reference size
$soc_{p,t}$	state of charge of storage technology p at time-step t
t	index of time-steps

T	set of time-steps
$V_{reactor}$	size of the reactor
$z_{p,t}^{ch}$	charging of storage technology p at time-step t
$z_{p,t}^{dis}$	discharging of storage technology p at time-step t

Units

bar	bar
$°C$	degrees Celsius
€	euro
J/mol	joule per mole
kg/s	kilograms per second
m	meter
m/s	meter per second
m^2	square metre
m^2	cubic meter
t	tonne
W	watt
Wh	watt-hour

Contents

List of Figures

List of Tables

1

Introduction

After the Paris Agreement, countries set out to aim for an average global temperature rise below 2 °C above pre-industrial levels, and to reinforce efforts to limit the temperature increase to 1.5 °C [1]. The aim of this treaty was to limit global warming by reducing greenhouse gas emissions, so as to minimize the impact of climate change. The largest share of carbon emissions per sector in 2021 came from the production of electricity and heat, which accounted for 40% of the CO_2 emissions worldwide with 14.6 Gt emitted, its highest level in history [2].

Regarding the electricity system, the rapid decline in the cost of renewable energy technologies over the last decade has promoted the introduction of variable renewable energy (VRE) to satisfy electricity demand [3]. However, the power generated by sources such as wind and solar photovoltaic depends upon the weather, thus providing a variable energy supply. Variation management strategies (e.g., energy storage, demand-side management, supply-side management, advanced energy conversion technologies, and grid infrastructure) are often highlighted as key enablers of managing variability, increasing the value of VRE and reducing energy curtailment [4–6].

With regards to the heat supply sector, biomass resources provide the main carbon-neutral solution for the residential heating sector (given they are widely available and sustainably managed). However, biomass is a limited resource needed in the transition of many sectors of the economy, such as in the chemical industry, where is used as feedstock for sustainable synthesis processes. Consequently, its future cost and availability are highly uncertain. In September 2022, the European Commission (EC) published a revised version of the Renewable Energy Directive of the European Union (EU), which limits the use of woody biomass for power generation. In addition, the EC requested excluding woody biomass from the calculation of the renewable energy share of EU member countries for the 2030 climate targets in order to move from neutral to negative in terms of CO_2 emissions [7]. This directive sets up a challenge for countries where district heating (DH) facilities are based on biomass-fired combined heat and power plants (CHPs). Large-scale biomass-fired DH plants typically use fluidized bed (FB) combustors, known to have large fuel flexibility [8]. This feature opens up the need for FB combustion plants to reconsider the energy source to be used, in the ideal case, these plants should make use of VRE. The question arises of how should these plants be transformed and whether it is possible to make a retrofit.

If combined with storage technologies, DH plants can act as energy buffers, thus aiding the penetration of VRE. The electrification of DH plants with thermochemical energy storage (TCES) has the potential to absorb non-dispatchable electricity from VRE sources and, thereafter, produce dispatchable DH and eventually, also electricity [9]. Some of the main advantages of TCES processes are the possibility of storing energy over months, the high temperature at which heat can be supplied (which depends on the chemical system used) and the possibility of reusing and retrofitting existing DH facilities.

Studies on the implementation of TCES processes can be found in the literature, techno-economic analyses on the large-scale implementation of these processes are scarce, though. For the specific case of DH production, no dedicated work is available that deals with issues such as the impact of the cost of electricity on the design of TCES processes, investment decision-making or the identification of barriers and opportunities. Understanding the cost-effectiveness of TCES technologies is essential for their development and deployment.

1.1 Aim and scope

The aim of the present work is to provide an economic assessment of implementing a TCES scheme in existing FB-based DH plants. The scheme selected for the study is electricity-charged and based on a metal-based solid cycle. To achieve the goal of this thesis, a series of specific objectives are defined.

- Develop the investment cost function of the retrofit.
- Study the impact of electricity price variations on the optimum investments in process equipment and storage capacities.
- Identify the implications of future volatile electricity prices for the cost of heat production.
- Estimate the economic indicators for the implementation of the suggested heat production process.

The geographical scope selected for the study is Sweden, which is of special interest because of the extensive use of biomass-fired plants for DH and the growing capacity of VRE generation. The existing infrastructure for iron extraction and processing in Sweden supports the availability of material to implement the TCES scheme. Nevertheless, the investigation carried out in this work is relevant to other countries with similar characteristics. The present thesis focuses on providing an economic assessment at a plant level. The temporal scope considered in this thesis is one year in a VRE-dominated electricity system.

2

Background

In Section 2.1 the description of the electricity-charged metal-based solid cycles used in the TCES process is introduced. Section 2.2 describes the Swedish DH system with a special focus on the plants based on biomass-fired FB boilers while Section 2.3 provides an overview of the Swedish iron and steel sector.

2.1 Thermochemical energy storage

Energy storage can be achieved in a variety of ways, such as mechanical, thermal or chemical energy storage. Chemical energy storage technologies, utilize a reversible reaction and accumulate the energy in the formation of strong chemical bonds [10]. Materials used in chemical energy storage processes achieve much higher energy storage capacity than mechanical and thermal energy storage technologies. 120-250 kWh/t can be achieved with chemical energy storage, while only 0.5-60 kWh/t and 10-150 kWh/t are achieved with mechanical and thermal energy storage, respectively [11, 12]. For the specific case of TCES systems, energy is both absorbed and released in the form of heat.

In a TCES system, there is one endothermic (energy absorption) and one exothermic (energy release) stage. Therefore, three main operational steps for TCES processes are identified: charging, storage and discharging. In Figure 2.1 a schematic of the implementation of a TCES process is provided. During the charging step, heat is stored in the material in form of chemical energy. The charging section can be considered a Power-to-X technology that has the potential to transform electricity into chemical energy, which is stored in the product material. During the discharging step, the energy stored is released in the form of heat at high temperatures (300°–1100°C, depending on the chemical system chosen) [13]. Therefore, the process has the potential to convert non-dispatchable into dispatchable energy.

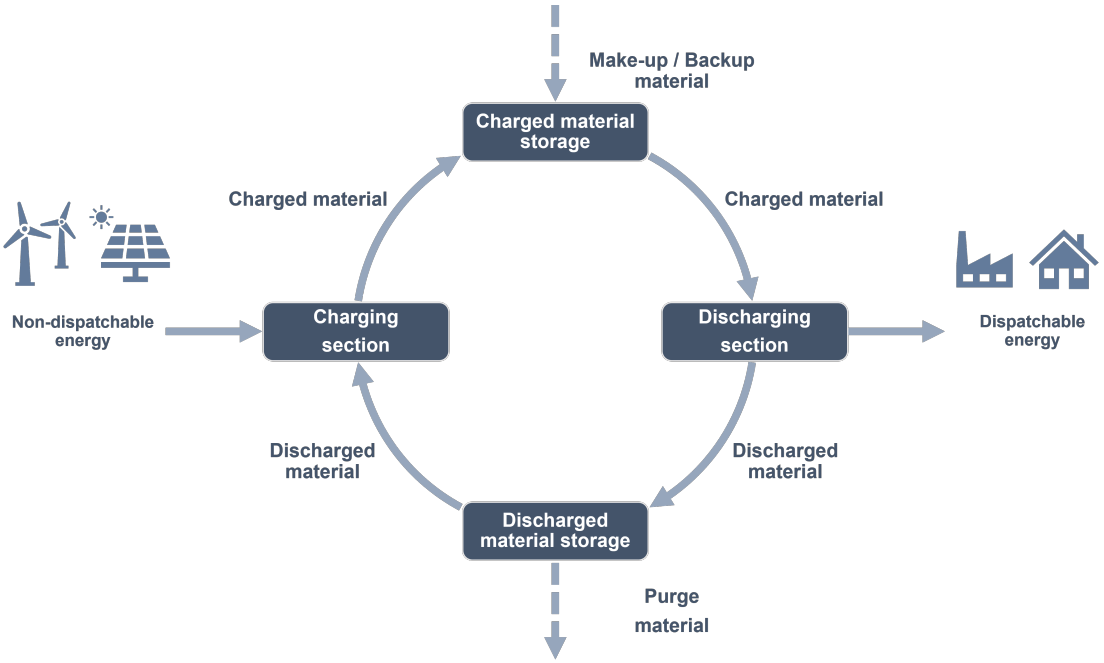

Figure 2.1: General schematic of a TCES process.

The main TCES systems can be grouped according to whether they are based on solid-gas or gas-gas reactions. Solid-gas reactions are often preferred over gas-gas reactions for implementing TCES systems because typically higher energy densities can be achieved and allow greater ease of storage [12, 14]. Carbonates, hydroxides, metal hydrides and metal oxides count among the different materials used in solid-gas TCES systems [14]. Carbonate looping (CaL) processes are based on the reversible carbonation reaction (CO_2 with a metal oxide e.g., calcium oxide (CaO) or magnesium oxide (MgO)), are positioned as an emerging technology for the decarbonization of fossil fuel power generation systems [9, 15, 16]. Other authors focus on TCES processes based on hydroxides, which use reversible hydration/dehydration reactions of metal oxides [17–19]. For large-scale power generation, TCES processes based on metal oxide redox systems are often highlighted as the most promising candidates due to the possibility to discharge the material at high temperatures (700°–1000°C), compared to systems based on hydroxides (400°-600°C) or metal hydrides (300°-600°C) [14, 20, 21].

When selecting a material for a TCES system for power generation, it is important to consider factors such as the material's ability to be stored for long periods of time at ambient conditions and its ability to be safely transported over long distances. Metal oxides meet these criteria. Among the pure metal oxides, cobalt oxide, iron oxide, copper oxide, and manganese oxide show suitable reaction temperatures, high reaction enthalpies, cycling stability, and low material costs [22]. Several authors have conducted studies on the implementation of TCES systems based on redox reactions using cobalt-iron (Co-Fe) and manganese-iron (Mn-Fe) mixed metal oxides [21, 23]. Bergthorson et al. have focused on analyzing dry metal-fuel cycles based on iron for stationary power generation. Iron is often suggested as a cost-effective

solution due to its high volumetric energy density, low market price, availability and already-existing infrastructure for its extraction and processing [11]. Additionally, iron powders are not toxic.

Studies focusing on the reduction of iron oxide particles with green hydrogen [24] and the retrofitting of combustors to process iron oxide particles [25, 26] support the technical feasibility of using iron oxide-based redox cycles with TCES. In order to fully understand the potential of TCES using iron oxide redox systems in future VRE-dominated energy systems, techno-economic analysis, as well as studies on the influence of the electrical system on the performance and operation of such systems are required.

A recent study by Guío-Pérez et al. proposes and evaluates a process for the implementation of electricity-charged iron oxide-based solid cycles with TCES in existing FB-based DH plants [27]. The results of the mass and energy balances showed that, at the plant level, the scheme proposed by the authors meets the heat demand of the DH while also enhancing the plant's capacity for the production of non-dispatchable heat. Such work analyses the operation under selected scenarios in terms of electricity price and electricity variations. While this approach provides valuable insights, it does not fully assess the impact of the electricity system variability on the cost-optimal sizing of the units that comprise the system studied.

2.2 Fluidized bed combustion plants with district heating production

In Sweden, the DH sector accounted for around 49 TWh of the total energy consumption in 2019, when considering both industrial and residential heat [28]. Figure 2.2, shows the different energy sources used in the production of DH in Sweden. 63% of DH in Sweden comes from biomass, in the form of pellets or wood chips. The use of heat pumps (HP) for DH has gained popularity over the past 20 years, due to their high efficiency and ability to be integrated into the already-existing DH infrastructure. Currently, 15% of the DH production comes from other fuels (i.e., peat or bio-oils) and 8% from waste heat. There is also around 6% of DH production coming from fossil fuels such as natural gas, petroleum products and coal. Thus, Sweden's DH system is dominated by biomass.

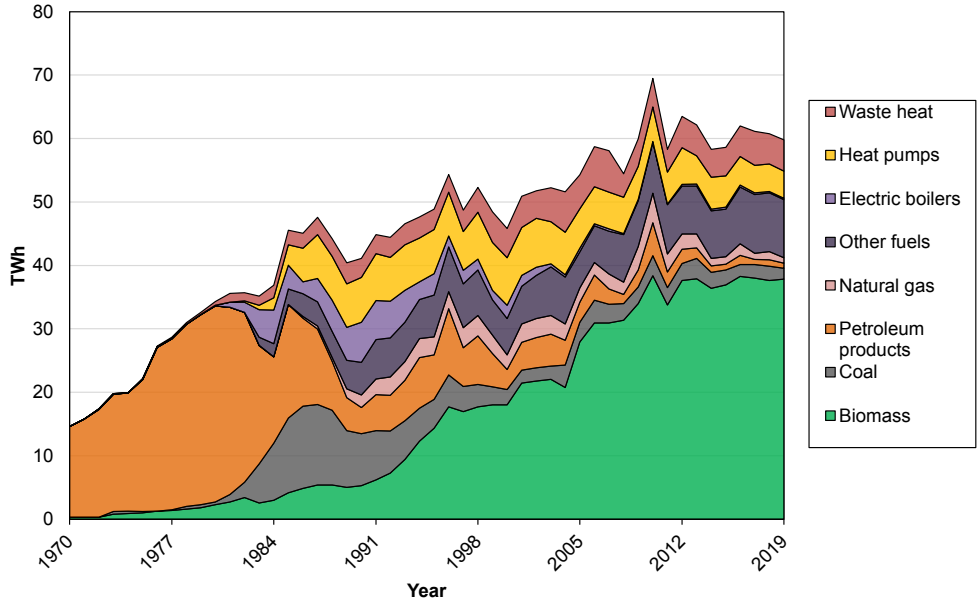

Figure 2.2: Input energy utilized in the production of DH in Sweden between 1970 to 2019. Adapted from [2].

As outlined in Section 2.1, TCES schemes are capable of releasing stored energy in the form of high-temperature heat. This characteristic makes it a highly suitable option for retrofitting existing DH plants, which are often based on biomass-fired FB combustors, which are a commonly used technology in the Swedish DH system. As of January 2016, Sweden had a total of 119 FB combustors installed, with a combined thermal capacity of 6920 MW [29]. Gothenburg, Sweden's second-largest city, can be considered a representative case of the Swedish DH system since it operates several DH plants based on biomass-fired FB combustors. Table 2.1 shows the plants that make up the Gothenburg DH system.

The leading supplier of the city is the municipal company Göteborg Energi, which operates several CHP plants, Högsbo kraftvärmeverk, Rya kraftvärmeverk, Rosenlundsverket and Sävenäsverket HP3 to generate both heat and electricity. The latter uses biomass as a fuel, as does Rya värmecentral, which uses a heat-only boiler to produce heat for the district heating network. Although the Rosenlundsverket plant has the highest installed power (776 MW), it cannot be considered a reference case of the biomass-dominated Swedish DH system due to its utilization of natural gas as a source of industrial heat for the nearby industries. The company also owns Rya värmepumpverk, a facility with two large-scale HP that use treated sewage water as their cold sides. Several small-scale heat generation plants are owned by Göteborg Energi in order to cover local peak loads.

The Rya plant, until March 2021, had two 55 MW fluidized bed boilers. In order to upgrade the plant, the two old units were replaced by a new 130 MW fluidized bed boiler [30, 31]. Sävenasverket HP3 is also operating with a FB boiler since biofuels were first used for heat production in the plant in 2004 [32]. The already-existing FB boilers with which these plants currently operate could be modified to process

metal powders [26]. As illustrated above, the standard capacity for these plants is around 100 MW thermal output. This size is used as the reference plant size in the current study (see Section 4.4).

Table 2.1: Heat generation plants in the current district heating system in Gothenburg. Eo1 is a fuel oil based on distillate, while Eo5 is a residual fuel oil. R-134a is the refrigerant used in the HP.

District heating plant	Max installed power (MW)	Max heat output (MW)	Max electrical output (MW)	Fuel
Alekärrsgatan	140	120	0	Natural gas
Angereds värmecentral	108	101	0	Bio-oil, Eo1
Backa panncentral	36	32	0	Eo1
Högsbo kraftvärmeverk	34	16	13	Natural gas
Margaretebergsgatao	0.08	0.078	0	Natural gas
Rosenlundsverket	776	670	36	Natural gas, Eo5
Rya kraftvärmeverk	600	294	261	Natural gas, Eo1
Rya värmecentral	110	100	0	Pellets, Natural gas
Rya värmepumpverk	55	160	0	Energy from waste water, electricity, R-134a
Sisjöns värmecentral	24	21	0	Natural gas, Eo1
Skarvik panncentra	13.5	11.6	0	Pellets, natural gas, Bio-oil
Sävenäsverket HP1	81	73	0	Natural gas, Eo1
Sävenäsverket HP2	89	80	0	Natural gas, Eo1
Sävenäsverket HP3	105	95	13	Wood chips, bio-oil
Tynnered panncentral	22	20	0	Eo1, Bio oil
Häljered panncentral	9	8	0	Electricity, Eo1
Skepplanda panncentral	3.3	2.3	0	Pellets, Eo1
Sörreds panncentra	170	155	0	Natural gas, Eo1, electricity

2.3 Swedish iron and steel industry

Sweden currently (2021) holds 60% of the known iron ore reserves in Europe and carries out 92% of iron ore extraction in Europe [33]. In Figure 2.3, the locations of current metal mines and concessions in Sweden are shown. Most of the country's mining operations are concentrated in the Lapland region in the North of the country hosting nine out of the twelve active Swedish mines.

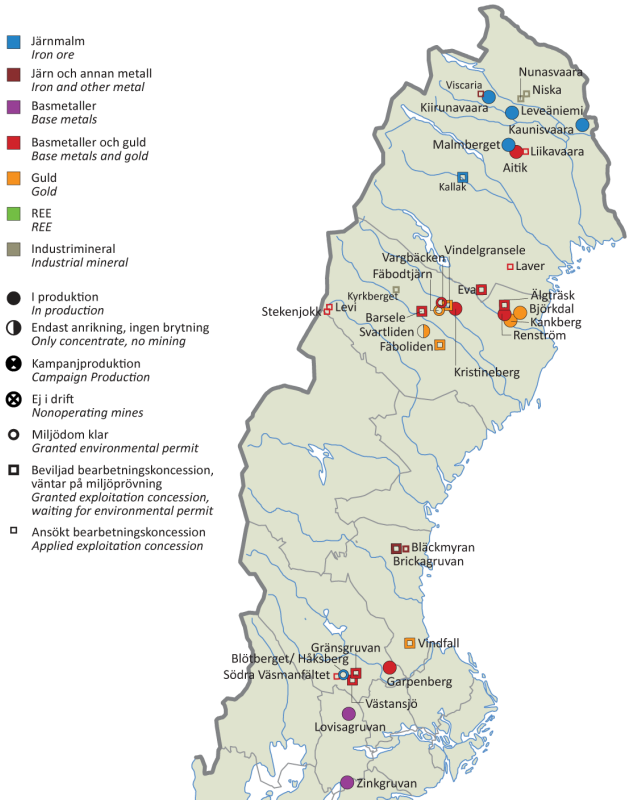

Figure 2.3: Location of current metal mines and concessions in Sweden. Reproduced from [34].

One of the major applications of mined iron ore is the production of steel. Two different steel production technologies are currently being used: the iron ore-based steelmaking process, which uses pig iron to obtain steel using blast furnaces (BF) or basic oxygen furnaces BOF, and the scrap-based steel production using electric arc furnaces (EAF) [35]. Fossil fuels, such as coal, coke, and natural gas are essential feedstock in the iron ore-based steel production process. The long-lived capital stocks and the process emissions make the iron and steel industry challenging to decarbonize.

Significant reduction of CO_2 emissions from the iron and steel sector can be achieved by either electrification, such as direct reduction with hydrogen, or by using carbon capture systems in combination with biomass. Sweden is currently focused on the direct reduction of iron ore [36]. Iron ore reduction with hydrogen is a process that involves reducing iron oxide ores to produce reduced iron using hydrogen as the reducing agent. The general idea is to use electricity from VRE sources to produce the hydrogen required for iron ore reduction through the electrolysis of water. The overall reaction, which begins with totally oxidized iron in the form of hematite (Fe_2O_3), is (a first step in which the magnetite present in the iron ore is oxidized to hematite is not presented here):

$$\begin{aligned} &\mathrm{Fe_2O_{3(s)} + 3H_{2(g)} \leftrightarrow 2Fe_{(s)} + 3H_2O_{(g)}} \\ &\mathrm{\Delta H_{298\ K,1bar}} = +100.7\ \mathrm{kJ/mol}. \end{aligned} \tag{2.1}$$

The reaction, in most cases, takes place stepwise. Hematite (Fe_2O_3) reduction to magnetite (Fe_3O_4):

$$\begin{aligned} &\mathrm{Fe_2O_{3(s)} + 1/3H_{2(g)} \leftrightarrow 2/3Fe_3O_{4(s)} + 1/3H_2O_{(g)}} \\ &\mathrm{\Delta H_{298\ K,1bar}} = +2\ \mathrm{kJ/mol} \end{aligned} \tag{2.2}$$

Magnetite (Fe_3O_4) reduction to wustite (FeO):

$$\begin{aligned} &\mathrm{Fe_3O_{4(s)} + H_{2(g)} \leftrightarrow 3FeO_{(s)} + H_2O_{(g)}} \\ &\mathrm{\Delta H_{298\ K,1bar}} = +58.5 - 70.1\ \mathrm{kJ/mol} \end{aligned} \tag{2.3}$$

Wustite (FeO) reduction to metallic iron (Fe):

$$\begin{aligned} &\mathrm{FeO_{(s)} + H_{2(g)} \leftrightarrow Fe_{(s)} + H_2O_{(g)}} \\ &\mathrm{\Delta H_{298\ K,1bar}} = +24.7\ \mathrm{kJ/mol} \end{aligned} \tag{2.4}$$

The process can be carried out using different technologies, such as a direct reduction shaft furnace, a rotary kiln or a FB reactor. The latter is of great use in multi-phase chemical reactions in technical fields like chemical and petrochemical processes, mineral and metallurgical processes, and electric power plants [37]. FB reactors are considered a suitable solution for the direct reduction of iron with hydrogen due to several benefits such as the capability to handle feedstocks of various particle sizes, as well as a high capacity good mixing and heat transfer [38].

In addition, iron ore reduction with hydrogen in FB reactors has the potential to be more energy-efficient and environmentally friendly than traditional methods of iron production, such as the blast furnace process, which uses coke as a reducing agent and emits carbon dioxide into the atmosphere. Although the technology is still in the development stage, Metso Outotec's Circored method is the only process for iron ore reduction based on 100% hydrogen that has proven its functionality and performance at MW scale [39, 40].

In the hydrogen direct reduction process the conversion of iron ore into direct reduced iron (DRI) is usually followed by the compression of DRI into hot briquetted iron (HBI). The main advantage of HBI is the significant decrease in reactivity compared to DRI, which allows the handling and storage of the material more safely [41].

3

Process description

As discussed in Sections 2.2 and 2.3, the reasons for considering iron oxide as the operating material in this thesis are the high volumetric energy density, low market price, availability, and existing infrastructure for extraction and processing of iron in Sweden. The process scheme proposed by Guío-Pérez et al. [27] is used as the basis for the process layouts investigated in this thesis. Section 3.1 describes the main process layout for the proposed TCES system based on iron oxide redox cycles for retrofitting existing DH plants. In Section 3.2 two additional process layouts for implementing the proposed TCES process are given.

3.1 Main process layout

The input to the proposed process absorbs non-dispatchable renewable electricity, which is used to produce the hydrogen required for the reduction of iron oxide. The energy is then stored in the form of reduced iron oxide material and can be delivered in the form of dispatchable heat. In the present work, the emphasis is placed on the assessment of the option of DH production, despite the possibility of providing combined heat and power.

Figure 3.1 shows the schematic of the so-called main process layout, where the charging and discharging sections are differentiated. A significant advantage of the main process layout is the availability of essential process equipment at a large scale. The process layout considers FB reactors for both reduction and oxidation reactors. The storage units at ambient conditions allow for the potential introduction of shipping of charged material and make-up streams into the process, as suggested in [27].

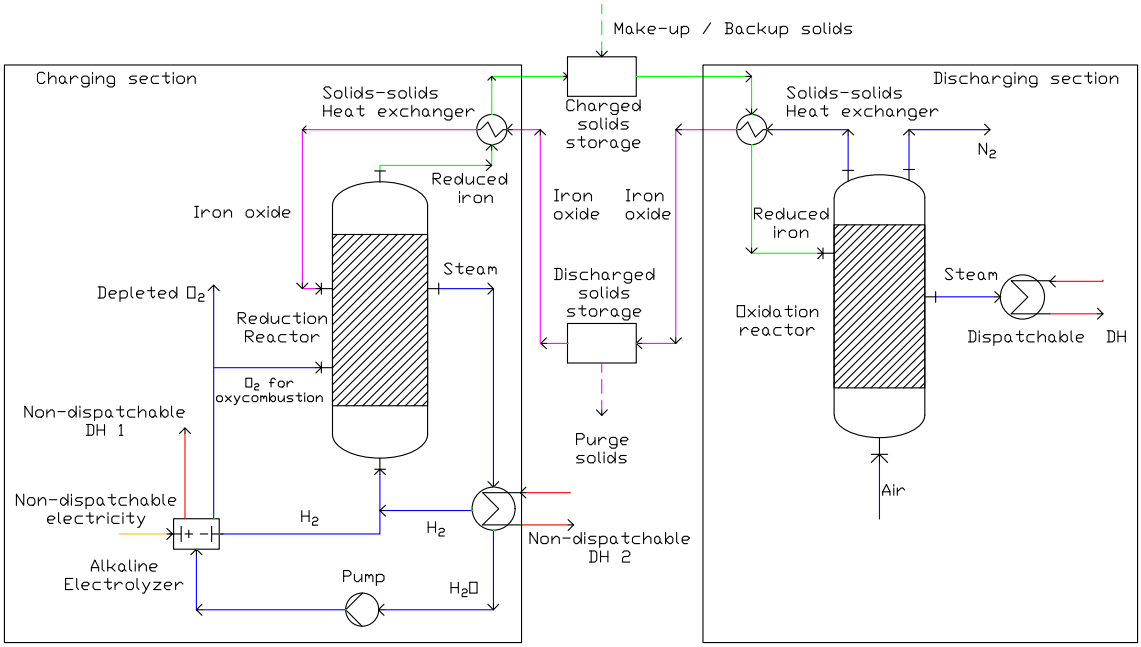

Figure 3.1: Main process layout for implementing electricity-charged iron-based solid cycles with TCES. Blue lines indicate fluids, green lines indicate reduced solids, and magenta lines indicate oxidized solids. Input electricity is depicted in yellow, and supplied heat is shown in red.

With regard to the operation of the plant, in the main process layout, the reduction and oxidation reactors are decoupled by incorporating solids storage units. This allows the plant to be designed in such a way that the charging section can operate following the electricity price variations, in order to charge the material during times of strong availability and competitive prices of renewable electricity. The process enables the recovery of waste heat from the charging section, which can be utilized to meet heat demand during peak periods. As stated by Guío-Pérez et al. in [27], the proposed scheme increases the plant heat generation capacity, allowing the possibility of using the oxidation reactor only during periods of high heat demand and unfavorable electricity prices.

The charging section of the plant includes an electrolyzer based on alkaline electrolysis cells (AEC), a reduction reactor and a HP. The electrolyzer, operated with non-dispatchable electricity, splits water and supplies hydrogen for the reduction reaction of iron oxide (see Section 2.3) that takes place in the reduction reactor. The operation of the charging section results in the production of non-dispatchable DH. Heat can be extracted and utilized in the form of DH by cooling and condensing the high-temperature steam that leaves the reduction reactor. The water outlet leaving the condenser is recirculated as the input for the AEC electrolyzer. Additional useful waste heat can be extracted from the process by utilizing the heat losses generated during the operation of the AEC electrolyzer (up to 18.4% of the net input, according to [42]) and upgrading the heat to DH-suitable temperatures using a HP. The DH supply temperature in the Swedish system is typically around 90 °C [43, 44].

Regarding the discharging section, the reduced material is fed from storage tanks into the oxidation reactor, where the air is used to fluidize the solid material and provide oxygen for the oxidation reaction. The heat produced during the reaction is used to generate steam for heat production according to conventional DH schemes. To minimize energy losses caused by storing solids at high temperatures, two solids-solids heat exchangers (SS-HX) are introduced into the layout, which allow the input solids streams to be preheated with the solids leaving the reactors.

According to the results of Guío-Pérez et al. [27], the conditions that favor a high conversion rate of the reduction are, a low reaction time of 100 min, a temperature of 1100°C and a pressure of 1 bar. Meanwhile, the operational conditions of the oxidation reactor were fixed at 900°C and 1 bar. The results from the authors of the chemical analysis of the solid streams showed that the oxidation reactor produced 100% Fe_2O_3, while the reduction reactor produced a mixture of FeO (74%) and Fe_3O_4 (26%). This suggests that metallic iron cannot be produced under the current reduction conditions. Therefore, the process investigated in this thesis involves the reduction-oxidation of iron oxide between its Fe_2O_3 and FeO (i.e., Equation 2.2 and 2.3).

The following subsections provide a more detailed description of each of the process units comprising the main process layout.

3.1.1 Alkaline electrolyzer

Water electrolysis is the most developed to date process for producing hydrogen from renewable electricity [45]. The basic operation principle of this technology consists of using electricity to separate water into oxygen and hydrogen gas, according to the following reaction:

$$2\mathrm{H_2O} \rightarrow 2\mathrm{H_2} + \mathrm{O_2} \tag{3.1}$$

Compared to polymer electrolyte membranes (PEM), and solid oxide electrolysis cells (SOEC), AEC are in a more advanced stage of development, with a technology readiness level of 9 [46, 47]. Due to the maturity of AEC technology and its commercial availability in MW-scale, it is considered for hydrogen production the main layout. Figure 3.2 shows the basic set-up of AEC for the production of hydrogen by electrolysis.

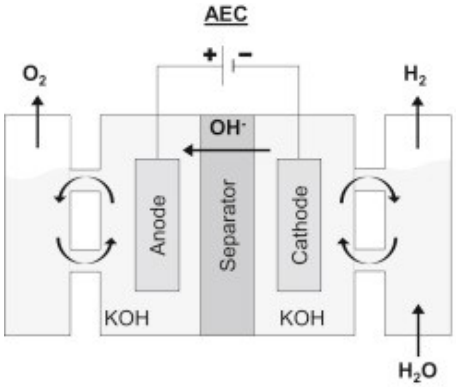

Figure 3.2: Schematic description of the electrolysis process in AEC electrolyzer. Reproduced from [48]

AEC electrolysis technology uses two electrodes submerged in a liquid alkaline electrolytic potassium hydroxide (KOH) solution [42]. Steel, nickel or nickel-plated steel are some of the materials from which electrodes are made. Electrons flow from the anode to the cathode, where they are consumed by H^+ ions to form H_2. Hydroxide ions (OH^-) are then transferred through the alkaline electrolyte solution from the cathode to the anode, where they are oxidized into oxygen and water [49]. AEC stacks operate at 65-90°C and can work at atmospheric pressure.

AEC electrolyzers require the inputs of electricity and high-purity water at a temperature of 25 °C and a pressure of 1 bar, while the outputs of this electrolysis technology are hydrogen, oxygen, and excess heat produced by the stack.

3.1.2 Waste heat recovery from the alkaline electrolyzer

Thermal losses from AEC electrolyzers can significantly impact the efficiency of the process, thus incorporating a waste heat recovery system is crucial for maximizing performance [42]. The waste heat recovery system proposed by Jonsson and Miljanovic [50] has been used as a reference. Figure 3.3 presents the design of the AEC waste heat recovery system. It consists of a cooling system and a HP that transmits the recovered heat to the DH system.

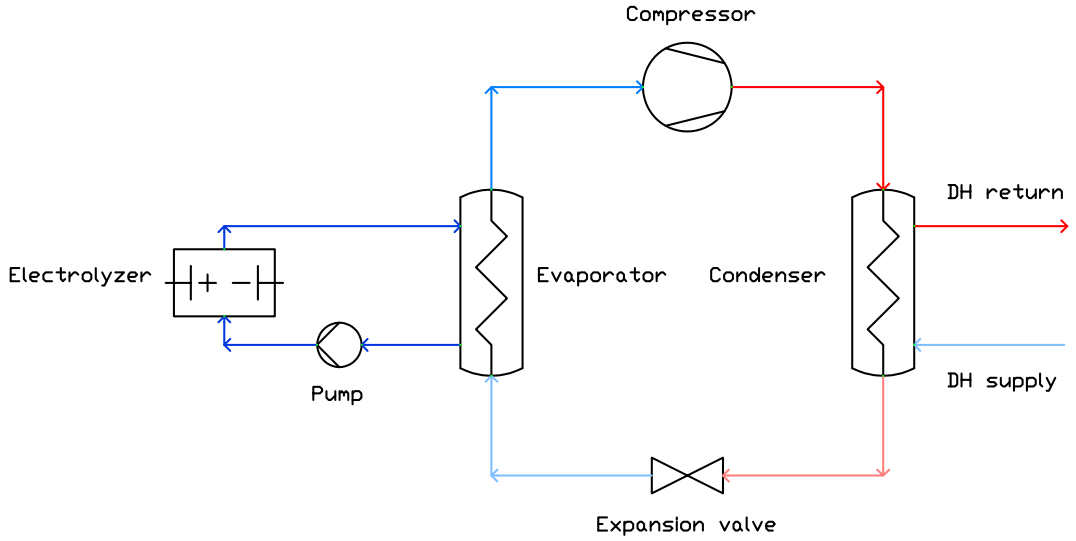

Figure 3.3: Schematics of waste heat recovery system for AEC with integrated DH production. Adapted from [50]

Coupling of electrolyzer to a variable electricity source implies large load gradients and changes in the rates of internal heat generation, leading to changes in the temperature profiles of the stack [51]. Therefore, thermal control within the electrolyzer has a significant impact on the AEC stack's overall performance. Although electrolysis is thermodynamically favorable at higher temperatures, the higher the stack temperature the greater the water loss due to evaporation and the more stringent demands for materials for the structural integrity of AEC [52]. The cooling system used in this work uses water as a refrigerant, which is circulated by a hydraulic pump.

To make better use of the heat dissipated by the AEC cooling system for the DH network, a HP is required so the temperature is increased to the level useful for DH. A HP, in its simplest structure, consists of 5 elements: the cooling fluid, an evaporator, a compressor, a condenser and an expansion valve. Heat extraction occurs when the refrigerant is at a lower temperature than the heat source and evaporates, thus absorbing heat. The refrigerant is then circulated to the compressor, where it is pressurized and its temperature is raised. The refrigerant then enters the condenser where condensation of the fluid occurs, thus yielding heat to the heat sink. Finally, the condensate passes through a valve that causes a pressure drop to the working value of the evaporator. The HP provides non-dispatchable heat to the DH system. Although additional elements and variations can be added to this simple scheme with the aim of improving cycle efficiency, in this study a single-stage HP cycle has been chosen to simplify the design.

3.1.3 Reduction reactor

FB reactors are industrial units employed in gas-solid operations. The FB consists of solid particles suspended in a gas stream, with the gas velocity high enough to cause the solid particles to behave like a fluid. This allows for efficient mixing and

high heat and mass transfer rates, making fluidized bed reactors an effective solution for processes such as gasification, combustion, and catalytic reactions [38, 53].

In the proposed process in this thesis, the iron ore reduction takes place in a FB reactor using hydrogen as the reducing agent. The iron ore is first preheated and then introduced into the reactor, where it is mixed with hydrogen gas. The hydrogen gas reacts with the iron oxide to form reduced iron oxide and water, according to the reactions presented in Section 2.3.

Due to the endothermic nature of the reduction reactions, energy is needed to maintain a constant temperature in the reactor. Mignard et al. explain that the reduction step requires as high a temperature as possible to ensure fast kinetics and a high conversion degree [54]. Spreitzer et al., after performing a multi-step kinetic analysis, conclude that the initial stage of reduction from Fe_2O_3 to Fe_3O_4, and partly to FeO, is controlled by diffusion and chemical reaction, which also depend mainly on the temperature [55].

To achieve the desired temperature, the electrolyzer must produce additional hydrogen (around 20% compared to the amount needed for the reduction [27]), so that the energy required by the reduction step can be supplied by the oxy-combustion of hydrogen. In this process, the additional hydrogen and some oxygen (also produced in the electrolysis) are mixed together in a burner, where they react to form steam and release heat.

3.1.4 Solids storage

Iron ore is a stable mineral and does not typically react with air or water at ambient temperatures and pressures. However, depending on the presence of impurities or the surrounding environment if the ore is exposed to high temperatures and pressures, such as in a fire, it may release flammable gases such as methane and carbon monoxide [56]. Iron ore can also be affected by moisture and if stored for a long time in a humid environment or in contact with water, it can become wet and heavy. This can cause problems in transportation and processing. Despite iron ore is typically stored in large stockpiles, in the proposed process the material is stored in a storage tank.

Unlike iron ore, for reduced iron open-air storage is not recommended [57]. Reduced iron is typically stored in a silo or dome before it is transported for processing. The silo or dome is designed to protect reduced iron from moisture and other environmental factors that could cause oxidation. Ideally, the material should be stored in an inert atmosphere, such as nitrogen, to further protect it from oxidation. Reduced iron that is stored in an inerted silo will lose very little metallization over the course of time [57].

3.1.5 Solids preheating

The studied process incorporates two SS-HX, which are used to preheat the input solids stream using the hot solids stream leaving each of the reactors. Although high-temperature TCES processes have not yet been fully implemented, it has been

assumed in the literature that the utilization of SS-HX technology is feasible and would enable the achievement of the necessary heat exchange rates. For instance, Martínez Castilla et al. in their study use SS-HX to reduce energy losses in the CaL process related to the storage being under ambient conditions [9]. Vorrias et al. propose a configuration of concentric L-valves as a solution for pre-heating the solids of the CaL process [58]. A schematic of this configuration is provided in Figure 3.4.

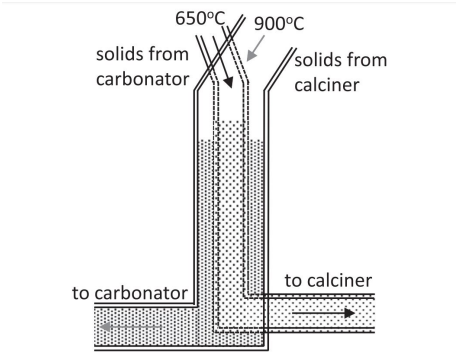

Figure 3.4: Schematic representation of a SS-HX. Reproduced from [58]

3.2 Additional process layouts

This section provides two additional implementation options and briefly introduces the components which vary from the main process layout.

3.2.1 Solid material and hydrogen storage

In this additional process layout, the AEC electrolyzer is decoupled from the reduction reactor through the implementation of hydrogen storage. Note that the reduction reactor remains decoupled from the discharging side as the solids storage is also in place. Although the main process layout has fairly good operational flexibility to adapt to changes in electricity prices, the additional storage may lead to a cost-optimal solution.

As shown in Figure 3.5, hydrogen is assumed to be stored in large-scale underground rock caverns. The hydrogen is stored in these caverns at high pressure, typically above 350 bar, to minimize its volume. This hydrogen storage system is considered safe and secure, as the solid rock formations provide a barrier against leaks and external threats such as fire or earthquakes [59, 60]. The introduction of hydrogen storage allows the electrolyzer to operate without the need to operate the reduction reactor.

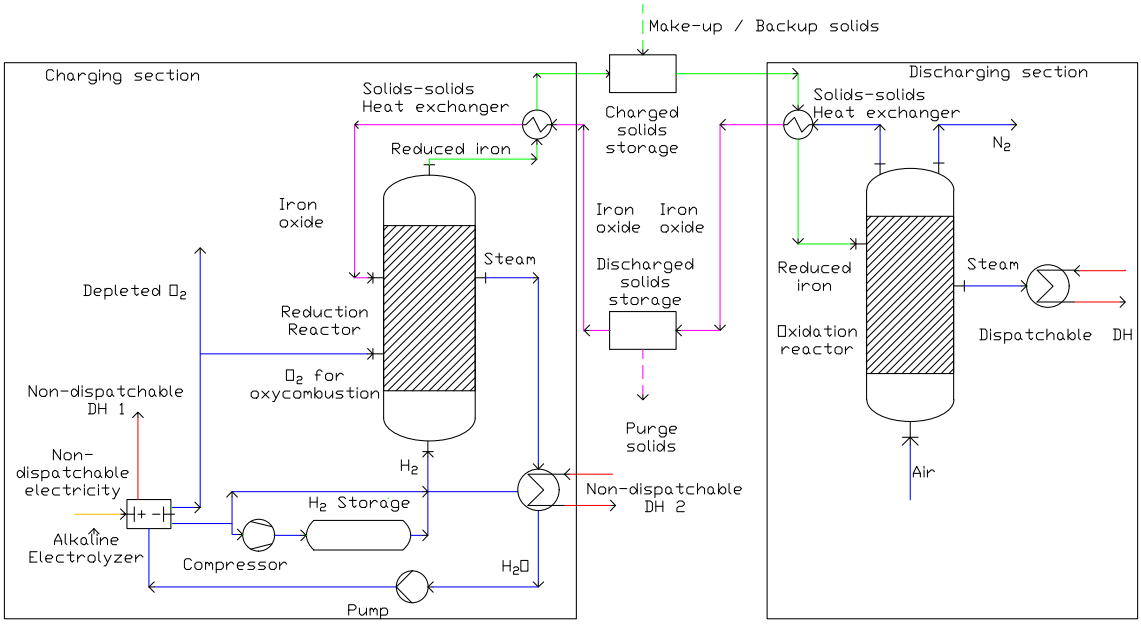

Figure 3.5: Additional process layout 1 - Solid material and hydrogen storage.

3.2.2 High temperature electrolyzer

The AEC electrolyzer is in this layout replaced with a high-temperature SOEC electrolyzer. SOEC electrolyzers operate at high temperatures (750-900°C), allowing them to accelerate the kinetics of the reactions that take place inside the cells and reduce the overpotential of the cathode and anode, thus lowering electrical consumption [61]. In the case of SOECs, the electrolyte is a dense ionic conductor consisting of ZrO2 doped with yttria-stabilized zirconia (YSZ) [62]. A combination of nickel and YSZ make up the cathode, while the anode is usually made of lanthanum strontium manganate (LSM) [42]. Due to the cell's solid ceramic design and the absence of liquid issues like corrosion are prevented, thus increasing the lifetime of the cells.

A schematic for this additional process layout, where TCES is implemented only in the form of solids storage, is presented in Figure 3.6. As opposed to AEC electrolyzers, SOEC electrolyzers consume not only electricity but also require a heat input, therefore recovery of waste heat from the electrolyzer is not considered in this technology and the only products are hydrogen and oxygen. The heat requirements of the SOEC electrolyzer can be supplied by the recirculation of the high-temperature steam flow from the reducing reactor into the electrolysis cells. This approach to heat integration leads to an improvement in the electrolysis efficiency of the SOEC electrolyzer, which can reach 87% as reported in [27].

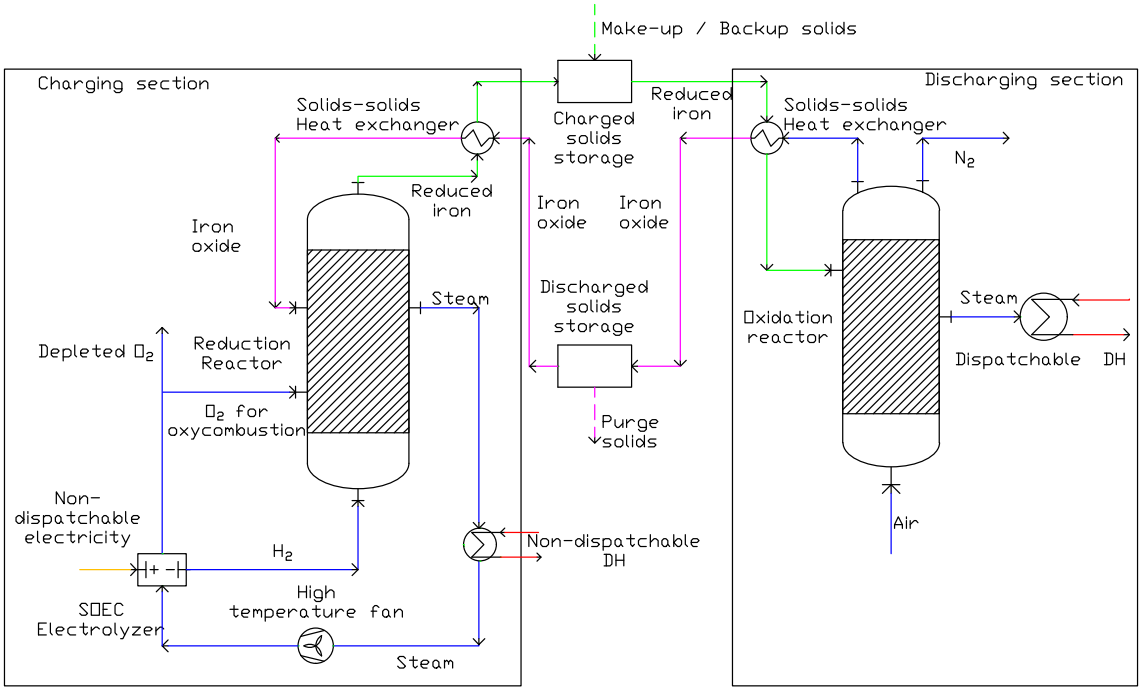

Figure 3.6: Additional process layout 2 - Solid material storage and SOEC electrolyzer.

4

Methods

The methodology developed and applied in this work is presented in Figure 4.1. The methodology is divided into three different stages, in which tasks are represented by green blocks in Figure 4.1. Two types of parameters are defined. The orange blocks represent varied parameters, which are systematically adjusted to represent a range of process layouts and configurations/mixes within the electricity system. Conversely, fixed parameters, which are extracted from previous works are represented by yellow blocks in Figure 4.1. Lastly, the grey blocks represent the output variables from each of the three stages. In the present study, various computing tools are utilized during the different stages. Microsoft Excel is used to characterize the capital expenditures (CAPEX) associated with the retrofit and to conduct the economic performance analysis, which involves the visualization of the final results. The cost-minimizing linear model is formulated and solved using General Algebraic Modeling System (GAMS).

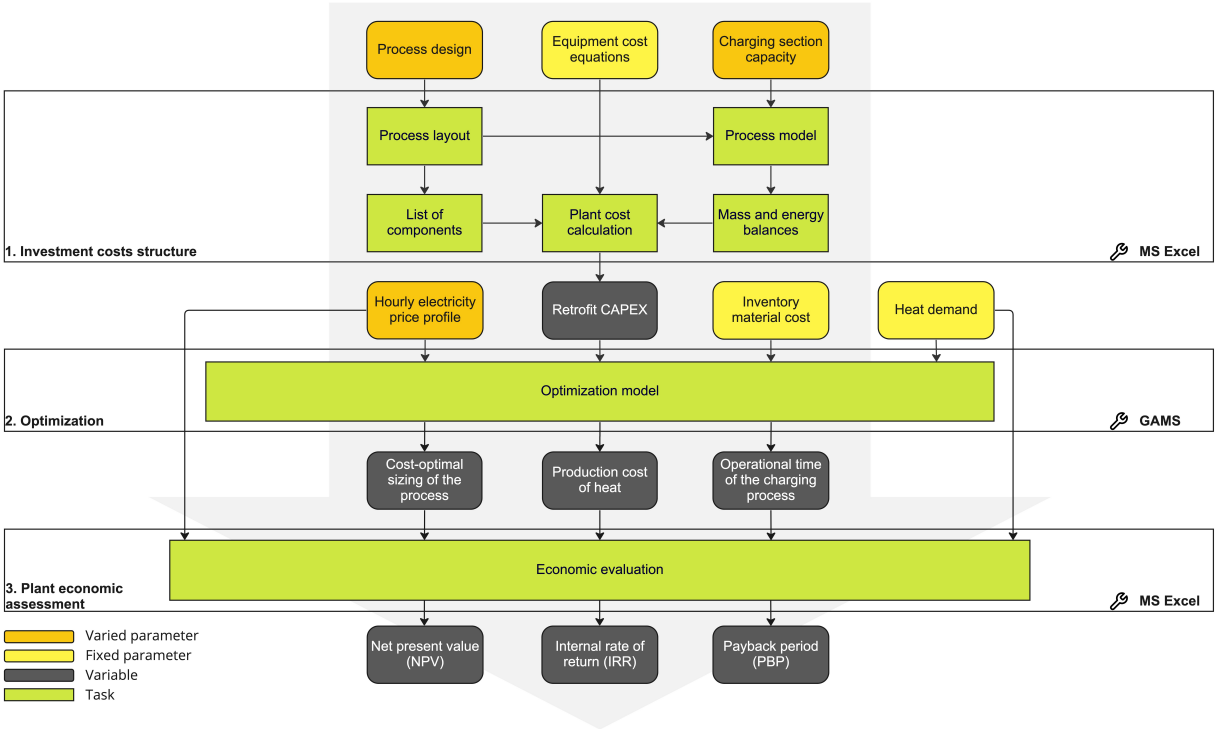

Figure 4.1: Scheme of the methods used in the study.

Section 4.1 describes the process followed for obtaining the investment cost function of the retrofit. Section 4.2 describes the linear cost optimization model used for the cost-optimal sizing of the process units. Section 4.3 focuses on the method to assess the economical performance of the process. Section 4.4 provides an overview of the input parameters considered for the work. Section 4.5 presents the scenarios studied in this work. Lastly, Section 4.6 presents sensitivity analyses of parameters with a high degree of uncertainty.

4.1 Investment cost structure

The initial stage of this thesis aims at quantifying the capital expenditure (CAPEX) associated with retrofitting existing biomass-based DH production plants with an iron oxide redox system with a TCES cycle. The methodology considers: (i) identifying and selecting the necessary equipment for the process; (ii) running an existing process model to compute the energy and mass balances [27]; (iii) obtaining the parameters for the preliminary unit sizing and cost evaluation. The procedure is completed for each of the process layouts proposed. While the size of the discharging section is fixed to the current size of the biomass boiler, the size of the charging section depends on the characteristics of the electricity input. Thus, for the generalization of the cost equation, different sizes of the charging section (in terms of electricity input) are evaluated. These values are extracted from the results of the study by Guío-Pérez et al. [27].

The bottom-up approach (BUA) methodology, by Manzolini et al. [63], is used to estimate the costs of the units of each process layout. This method, presented in Table 4.1, is used to obtain the total plant cost (TPC) of a given process layout from the BEC of the different units, by estimating aspects such as installation costs or contingencies with factors.

Table 4.1: Bottom-up-approach (BUA) cost estimation methodology. Adapted from [63]

Methodology for calculations of the TPC	**Cost**
Plant component	
Component X	X
Component Y	Y
Bare Erected Cost (BEC)	*X+Y*
Direct costs as percentage of BEC	
Total installation cost (TIC)	80% of BEC
Total Direct Plant Cost (TDPC)	*BEC+TIC*
Indirect costs (IC)	14% of TDPC
Engineering procurement and construction (EPC)	*TDPC+IC*
Contingencies and owner's cost	
Contingency	10% of EPC
Owner's cost	5% of EPC
Total contingencies and owner's cost (C&OC)	*15% of EPC*
Total plant cost (TPC)	***EPC+C&OC***

The investment cost function of the process depends on the BEC of the involved process components. The cost-to-capacity method and scale factors are a widely used approach for estimating the BEC of industrial plants and equipment [64]. This method is based on Equation 4.1, which utilizes a reference size (S_0), reference cost (C_0), and scale factor (f) as the basis for deriving specific cost equations.

$$C = C_0 \left(\frac{S}{S_0} \right)^f \tag{4.1}$$

While for mature technologies, a wide range of cost equations is available in the literature, less conventional equipment (such as the reduction reactor in this process) requires the development of a dedicated cost function. The following sections will detail the process of obtaining the cost equation for a FB reactor used in reducing iron ore with hydrogen, and provide a list of the equations used for the other components.

4.1.1 Reduction reactor

The literature presents a limited number of equations for estimating the costs of FB reactors for the reduction of a solid phase. For instance, the equation proposed by Flegkas et al. [17] for the reaction system $MgO/Mg(OH)_2$, which is derived from [65], only considers the cost of the pressurized vessel made of carbon steel. While, the

equation presented in [66] by Turton, provides cost estimations for process vessels, its upper limit of applicability, related to the size of the reactor, makes it inapplicable to the case studied in this thesis [66]. Furthermore, Woods in [67] describes two types of reactors for reduction/calcination reactions with FB reactors, but it only provides an equation for the one that processes small mass flows with high solid residence times, which is not relevant to the current case, thus it is also discarded [67].

The present work aims at developing an equation for estimating the BEC of the reduction reactor using the method depicted in Equation 4.1. The required parameters for the characterization of the expression (S_0, C_0 and f) are obtained from the financial data of the GoBiGas plant [68]. The main unit of the plant, a FB gasifier, has similar design characteristics as the FB reactor used in the process being evaluated in this thesis. More information about the GoBiGas project and the reference reactor can be found in Appendix A. Equation 4.2 is the resulting expression from the characterization. The size of the reactor ($V_{reactor}$) is determined by the solid material stream entering the reactor and the particle residence time. The method for determining the reactor volume is included in Appendix A.

$$C = 1161906 \cdot \left(\frac{V_{reactor}}{42.41}\right)^{0.70} \tag{4.2}$$

4.1.2 Other components

The cost equations for the remaining components have been obtained from the literature. The cost of each of the SS-HX is estimated using the cost equation of two FB dryers, as suggested in [9]. Table 4.2 summarizes the cost equations used in this work and their sources.

Table 4.2: Bare-erected cost functions (in M€) of the equipment used in the study. Heat flows are given in [MWth], diameters in [m], velocities in [m/s], areas in [m^2], pressures in [bar], volume of reactor and steel in [m^3], volume of hydrogen in [MWh], mass flows in [kg/s], electrical powers in [kW], and mechanical works in [MW].

Equipment	**Cost**	**Reference**
Electrolyzer	$C = 6.5 \cdot P_{elec} \cdot 10^5$	[42]
Heat pump	$C = (0.53 \cdot Q_{hp}) \cdot 10^6$	[69]
Reduction reactor	$C = 1161906 \cdot \left(\frac{V_{reactor}}{42.41}\right)^{0.70}$	[70]
Solids-solids heat exchanger	$C = 2 \cdot 3.5 \cdot 10^{-1} \cdot \left(\frac{D_b \cdot u_g}{2}\right)^{0.73}$	[67]
Cooler	$C = (2546.9 \cdot A_{HX}^{0.67} \cdot P_{\text{fluid}}^{0.28}) \cdot 10^{-6}$	[71]
Condenser	$C = (2546.9 \cdot A_{HX}^{0.67} \cdot P_{\text{fluid}}^{0.28}) \cdot 10^{-6}$	[71]
Pump	$C = \left(\frac{P_{pump}}{197}\right)^{0.60}$	[71]
Solids storage	$C = V_{steel} \cdot C_{steel}$	[72]
Hydrogen storage	$C = 11000 \cdot V_{H_2}$	[60]

4.2 Linear cost optimization model

To investigate the impact of the electricity price variations on the optimal size and operation of the electrified DH plant with TCES, a cost optimization model was formulated based on the one from Toktarova et al. [73]. The overall objective of the developed linear model is to minimize investments in heat production capacities (both dispatchable and non-dispatchable) and storage technologies (solids storage and hydrogen storage) while also minimizing the operating costs of the electrified DH plant with TCES, all while ensuring that the heat demand is met. It also provides the operational times and operational levels of all the plant units. The model developed has an hourly resolution and a temporal scope of one year

All sets, parameters and variables shown in this section are listed in Table 4.3. The main decision variables are: heat production capacity (i_p); production ($g_{p,t}$); and storage charge ($z^{ch}_{p,t}$) and discharge ($z^{dis}_{p,t}$). The set p represents the heat production capacities (electrolyzer waste heat recovery, reduction reactor heat recovery, oxidation reactor) and storage technologies (hydrogen storage, reduced solids storage, oxidized solids storage). The set t is time-step.

Table 4.3: Notations for the model description.

Sets	
T	set of time-steps
P	set of all technologies
P^{hpr}	subset of P that includes all heat production technologies (electrolyzer, reduction reactor, oxidation reactor)
P^{str}	subset of P that includes all storage technologies (hydrogen storage, reduced iron storage, iron oxide storage)
Variables	
C_p^{inv}	investment cost of technology p
$C_p^{O\&M,fix}$	fixed operating and maintenance cost of technology p
$C_{p,t}^{run}$	running cost of technology p in time-step t
C^{tot}	total heat production cost
i_p	capacity investment of in technology p
$g_{p,t}$	generation of heat and production of commodities of technology p at time-step t
$soc_{p,t}$	state of charge of storage technology p at time-step t
$z_{p,t}^{ch}$	charging of storage technology p at time-step t
$z_{p,t}^{dis}$	discharging of storage technology p at time-step t
Parameters	
D_t^{heat}	heat demand at time-step t
e_p	efficiency of storage technology p

The total heat production cost (C^{tot}) is calculated as the sum of the cost of investment (C_p^{inv}), the fixed operating and maintenance cost ($C_p^{O\&M,fix}$) and the running cost($C_{p,t}^{run}$). The total heat production cost, which should be minimized, can therefore be written as:

$$\min C^{tot} = \sum_{p \in P} (C_p^{inv} + C_p^{O\&M,fix}) + \sum_{p \in P} \sum_{t \in T} C_{p,t}^{run} g_{p,t} \tag{4.3}$$

To ensure that heat demand (D_t^{heat}) is satisfied at every time-step t, the constraint indicated in Equation 4.4 is added. In Section 4.4 the hourly distribution of the heat demand used for the cost optimization is provided.

$$\sum_{p \in P^{hpr}} g_{p,t} \geq D_t^{heat} \tag{4.4}$$

Equation 4.5 describes the utilization of storage units, i.e., the levels of materials

(hydrogen, reduced iron, oxidized iron) stored using the storage technologies at every time-step ($soc_{p,t}$).

$$soc_{p,t} = soc_{p,t-1} + e_p z^{ch}_{p,t} - z^{dis}_{p,t}, \quad \forall p \in P^{str}, \forall t \in T \tag{4.5}$$

Where $z^{ch}_{p,t}$ represents the amount of material charged to the storage at every hour t, $z^{dis}_{p,t}$ is the amount of material discharged from the storage, and η_p is the efficiency of the storage. In addition, the levels of products (hydrogen, reduced iron, oxidized iron) stored using the storage technologies have to be lower or equal to the storage capacity (i_p) at all times (Equation 4.6).

$$soc_{p,t} \leq i_p, \quad \forall p \in P^{str} \tag{4.6}$$

4.3 Process economic performance

An economic assessment is conducted based on the results obtained from the optimization model (see Section 4.2). In order to provide an evaluation of the financial viability of the investment, this assessment includes the revenues from heat generation. The key indicators used to evaluate the profitability of the process are: (i) Net present value (NPV); (ii) Payback period (PBP); and (iii) Internal rate of return (IRR).

The NPV is a financial indicator used to evaluate the absolute profitability of an investment. As seen in Equation 4.7, it is the sum of the present values of all cash flows generated by the investment over a time horizon. If the NPV is positive, the investment is considered profitable; if it is negative, the investment is not considered profitable.

$$NPV = \sum_{n=1}^{N} \frac{CF_n}{(1+r)^n} \tag{4.7}$$

The IRR is a financial indicator used to evaluate the relative profitability of an investment. It represents the annualized rate of return for a project or investment, taking into account the time value of money. IRR is the discount rate that makes the net present value (NPV) of all cash flows from a particular project equal to zero. A higher IRR indicates a more profitable investment and it is computed according to Equation 4.8

$$0 = \text{NPV} = \sum_{n=1}^{N} \frac{CF_n}{(1+IRR)^n} - CF_0 \tag{4.8}$$

The PBP is a measure of the time it takes for an investment to recover its initial cost. It is calculated by dividing the initial cost of the investment by the annual cash flow generated by the investment.

4.4 Input data

As outlined in Section 4.1, the first stage of the methodology requires a preliminary sizing of the process units in order to characterize the CAPEX equation of the retrofit. The details of this preliminary sizing can be found in Appendix A, which includes the coefficients and variables used. To ensure that the CAPEX equation for the retrofit is not based on arbitrary points, the plant size values presented by Guío-Pérez et al. in their study are taken into consideration for the preliminary sizing and evaluation of the cost equations [27].

Regarding the heat demand assumed for performing the cost-optimal sizing, the reference plant used is considered to represent a 100 MW unit of a municipal DH system (see Section 2.2). As shown in Figure 4.2, this work assumes that the electrified DH plant will operate at maximum capacity throughout the year except during the summer months, when heating is not required. Although the heat demand only has to be satisfied for 6569 hours, it is possible that the process operates the charging step during the months when no heat is to be supplied.

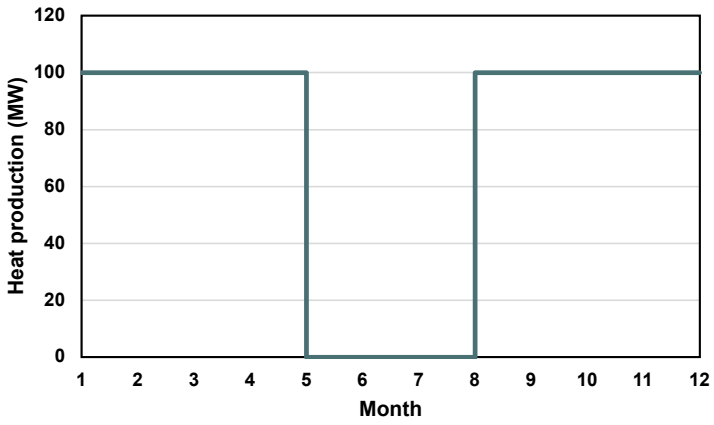

Figure 4.2: Heat demand profile assumed in this work.

The average sales price of DH for municipality-own DH systems is SEK 880 SEK/MWh, according to [74]. This value results in 72.8 €/MWh, according to the currency exchange used in this work for the Swedish krona. The selling price of heat is used to compute plant revenues in the process of economic performance analysis using the methods presented in Section 4.3. The nominal discount rate used for this work is 4.75 % and the lifetime of the plant is 20 years, according to the values recommended by [75].

The initial inventory for the commissioning of the plant is assumed to be 100 % in the form of reduced iron oxide, as the material is already charged and ready to be oxidized in the discharging section. The inventory of reduced solids required can be considered an investment cost since it is a material that can be cycled and used over a long period of time. The value of HBI is taken as the reference cost of the iron oxide material to be purchased. Although this value varies depending on origin and product quality, the global market price for HBI is between 250-300 €/t [76, 77].

In order to account for the purge and a make-up stream of solid material that are required owing to the expected loss of reactivity of the stored solid material [27], an efficiency of storage (η_p) of 99 % is considered.

4.4.1 Electricity price profiles

With the purpose of assessing the impact of electricity price variation on the design and operation of the plant, the optimization model is run using different price profiles. Three different electricity price profiles of Southern Sweden for three different years (2030, 2040 and 2050) were selected. The future electricity price profiles are obtained from a model called Hours-to-Decades (H2D), developed by Göransoson et al [5]. The H2D model is a cost-minimizing electricity system investment model that uses a semi-heuristic approach.

In the H2D model, the cost of carbon dioxide is assumed at 40 €/t in 2030, increasing to 100 €/t in 2040 and reaching 400 €/t in 2050 to incentive a complete removal of carbon dioxide emissions from the electricity system. It should be noted that the electricity prices from the H2D model, which in this work are used as a proxy for future electricity prices, reflect marginal costs of electricity generation and not the price formation on the market.

According to the results from the H2D model, the share of wind power in the electricity mix in Southern Sweden increases from 30% in 2030 to 65% in 2050. Furthermore, the model predicts that the average electricity price for the years 2030, 2040, and 2050 will be 33.1 €/MWh, 49.3 €/MWh, and 50.7 €/MWh respectively.

Figure 4.3 presents the electricity price duration curves for the three different electricity price profiles considered. As depicted in the figure, the increased penetration of wind power in the electricity mix will result in more frequent high- and low-price electricity periods.

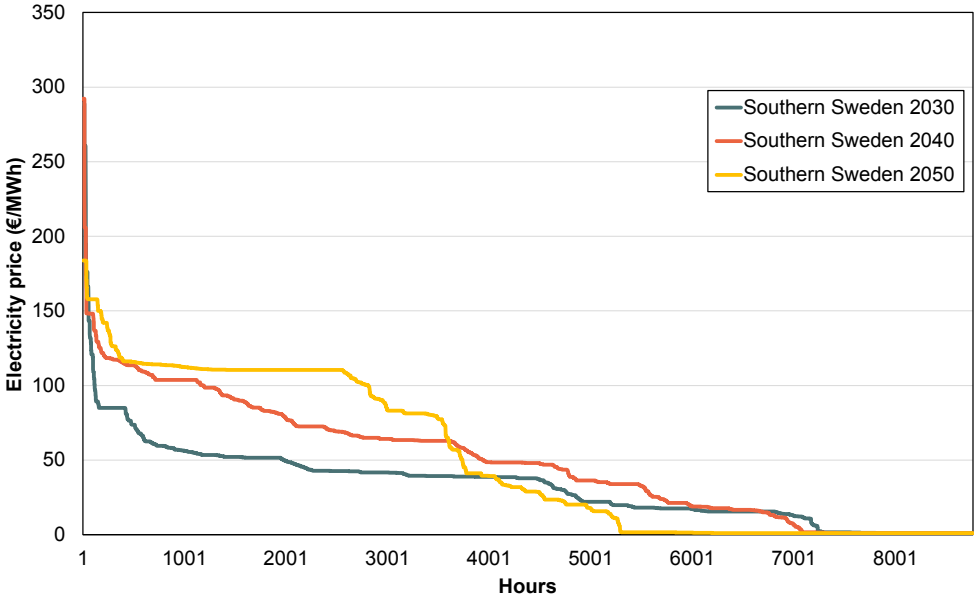

Figure 4.3: Electricity price duration curves for Southern Sweden in year 2030, 2040 and 2050

4.5 Scenarios description

To study the impact of both the process layout and the electricity price profile, twelve different scenarios are proposed. Table 4.4 provides an overview of the parameters that define the scenarios applied in the cost optimization model. The cells of the table representing the varied parameters are marked with two colors to indicate that the analysis takes into account the designated process layout (blue) and electricity pricing profile (yellow). The scenarios without storage of solids or hydrogen (*No_st_alk_2030*, *No_st_alk_2040* and *No_st_alk_2050*) represent the minimum investment level required for heat production units to meet the annual heat demand, assuming that the iron oxide redox system operates in a continuous loop without any storage capacity.

Table 4.4: Schematic overview of the parameters that define the investigated scenarios.

Scenario name	Process layout				Electricity price profile		
No_st_alk_2030	**No storage**	Only solids storage	Solids + H2 storage	SOEC Electrolyzer	**2030**	2040	2050
No_st_alk_2040	**No storage**	Only solids storage	Solids + H2 storage	SOEC Electrolyzer	2030	**2040**	2050
No_st_alk_2050	**No storage**	Only solids storage	Solids + H2 storage	SOEC Electrolyzer	2030	2040	**2050**
Solids_alk_2030	No storage	**Only solids storage**	Solids + H2 storage	SOEC Electrolyzer	**2030**	2040	2050
Solids_alk_2040	No storage	**Only solids storage**	Solids + H2 storage	SOEC Electrolyzer	2030	**2040**	2050
Solids_alk_2050	No storage	**Only solids storage**	Solids + H2 storage	SOEC Electrolyzer	2030	2040	**2050**
H2_solids_alk_2030	No storage	Only solids storage	**Solids + H2 storage**	SOEC Electrolyzer	**2030**	2040	2050
H2_solids_alk_2040	No storage	Only solids storage	**Solids + H2 storage**	SOEC Electrolyzer	2030	**2040**	2050
H2_solids_alk_2050	No storage	Only solids storage	**Solids + H2 storage**	SOEC Electrolyzer	2030	2040	**2050**
Solids_soec_2030	No storage	Only solids storage	Solids + H2 storage	**SOEC Electrolyzer**	**2030**	2040	2050
Solids_soec_2040	No storage	Only solids storage	Solids + H2 storage	**SOEC Electrolyzer**	2030	**2040**	2050
Solids_soec_2050	No storage	Only solids storage	Solids + H2 storage	**SOEC Electrolyzer**	2030	2040	**2050**

4.6 Sensitivity analyses

4.6.1 Inventory material cost

The cost of inventory material is an uncertain parameter. To address the potential impact of inventory material price variations on the cost-optimal size of the process studied in the present work, a sensibility analysis is conducted. For this purpose, the cost of inventory material is varied within a range from 0 €/t to 1200 €/t.

4.6.2 Bare-erected cost of the high-temperature electrolyzer

The sensitivity analysis of the BEC of the SOEC electrolyzer aims to assess the effect of its cost evolution in the next few decades and make a more equitable comparison to the AEC electrolyzer. In the sensitivity analysis, the BEC of the SOEC electrolyzer is varied between the values provided in Table 4.5 and extracted from the predictions for future costs from [42].

Table 4.5: Values considered for the BEC of a SOEC Electrolyzer in the sensitivity analysis. For the BEC values, the current cost of SOEC electrolyzers (2020), the predictions for future costs (2050) and the current cost for AEC electrolyzers (2020) are considered [42].

BEC (€/kW of total input)		
SOEC 2020	SOEC 2050	AEC 2020
4491	783	650

4.6.3 Discount rate

In order to evaluate the impact of the discount rate on the economic performance of the process, a sensitivity analysis is conducted. The discount rate is varied from 0% to 15% in increments of 1%. This range is chosen to cover a wide range of possible discount rates and provide an understanding of how the discount rate affects the NPV of the process.

5

Results and discussion

The results are presented and discussed in five different sections. First, Section 5.1 shows the cost-optimal sizes of the electrified DH plant units under the different investigated scenarios. In Section 5.2 the heat production cost for the different scenarios is presented. The results from the sensitivity analyses are presented in Section 5.3. Lastly, Section 5.4 provides the results of the economic performance analysis of the investigated process.

5.1 Sizing and investment cost

Figure 5.1 displays the results of the cost-optimal sizes of the different units in the electrified DH plant and under the investigated scenarios outlined in Section 4.5. Sizes are given in terms of capacity (electrolyzer and HP in MW, reduction and oxidation reactors in t/h of solids, reduced and oxidized metal storage units in kt of stored material) and compared against the process layout without any storage, which represents the minimum investment level required to meet the annual heat demand.

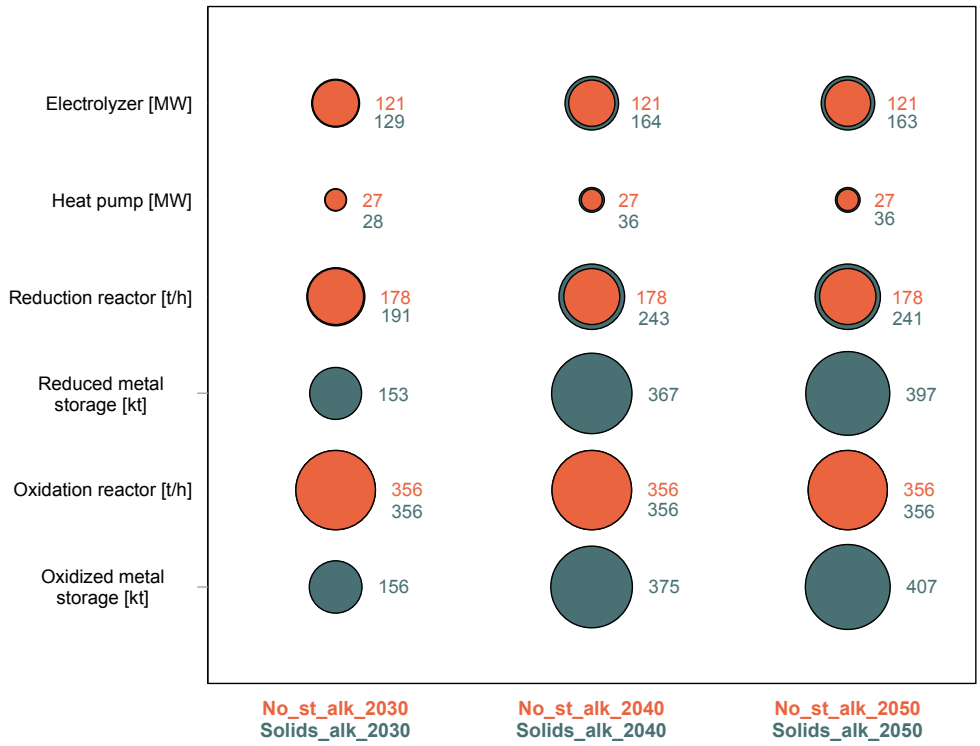

Figure 5.1: Cost-optimal sizes of the different units in the retrofitted plant for the investigated scenarios. The electrolyzer and HP sizes are expressed in MW, the oxidation and reduction reactors' sizes are in t/h of solids and the oxidized and reduced metal storage are in kt of stored solids.

As can be seen in Figure 5.1, introducing energy storage in the process (scenarios *Solids_alk_2030*, *Solids_alk_2040* and *Solids_alk_2050*), forces an overcapacity of the charging section (i.e., electrolyzer, HP and reduction reactor). For the *Solids_alk_2030* scenario, the charging section units are 7 % larger than in the *No_st_alk_2030* scenario, i.e., the minimum investment level. In the *Solids_alk_2050* scenario, the charging section units are 34 % larger compared to the minimum investment level, represented by the *No_st_alk_2050* scenario.

Analyzing the *Solids_alk* scenarios alone, it can be seen that the size of the reduced and oxidized metal storage units increases by 167 % between 2030 and 2050. At the same time, the size of the charging section units (i.e., electrolyzer, HP and reduction reactor) in the *Solids_alk* scenarios increases by 27 % between 2030 and 2050. This indicates that the increase in the variability of electricity prices adds overcapacity in the built equipment as well as in the material inventory within the plant.

The results for the *H2_solids_alk* scenarios reveal that the cost-optimal size of the hydrogen storage technology is zero, while the sizes of the other units remain unchanged compared to the *Solids_alk* scenarios. This means that the cost of hydrogen storage is too high to be compensated by reducing other capacities in the plant. Therefore the *H2_solids_alk* scenarios are not included in Figure 5.1. When evaluating the *Solids_soec* scenarios, it can be seen that the cost-optimal size of both the charging section and storage units is zero, meaning that the oxidation re-

actor is operated as an open-loop system and the operating material (reduced iron) is purchased to meet the heat demand. This operational mode does not follow the proposed scheme in this thesis, therefore the results for the *Solids_soec* scenarios are not depicted in Figure 5.1 either.

The required investment costs (CAPEX) of *Solids_alk_2030*, *Solids_alk_2040* and *Solids_alk_2050* scenarios are presented in Figure 5.2. The CAPEX is divided into the costs of inventory material and equipment. The highest investment cost in all the investigated scenarios is that of the electrolyzer, which accounts for 69 % of the total investment costs of the retrofitted DH plant. For the *Solids_alk_2030* scenario, the cost of the inventory material constitutes 20 % of the total CAPEX of the retrofitted DH plant, while for the *Solids_alk_2050* scenario, which presents the highest level of variability in electricity prices, the share of the CAPEX attributed to the cost of inventory material increases to 34 % over the total investment costs. This shows that large fluctuations in the electricity price lead to increased investments in inventory material.

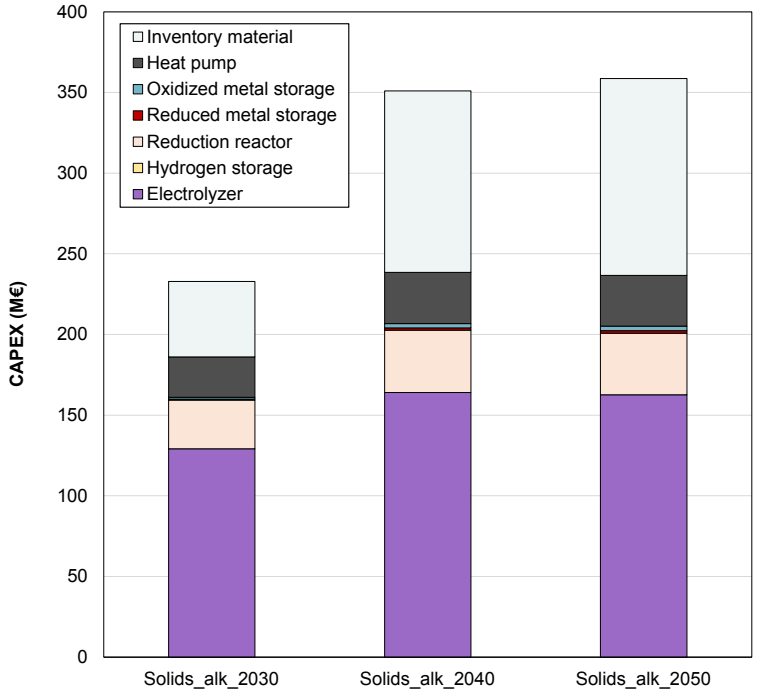

Figure 5.2: CAPEX breakdown into inventory material and equipment costs for the Solids_alk scenarios. Note that a size of 100 MW is assumed for the plant retrofitted with the main process layout

5.2 Heat production cost

Figure 5.3 shows the heat production cost as the sum of the inventory material cost (CAPEX), the equipment cost (CAPEX), the fixed O&M costs (CAPEX) and the cost of electricity (OPEX) for six different scenarios presented in Section 4.5. All

parts of the heat production cost are expressed per tonne of heat produced (i.e., €/MWh). Figure 5.3 compares the scenarios with solids storage (*Solids_alk_2030*, *Solids_alk_2040* and *Solids_alk_2050*) to the scenarios without any form of storage (*No_st_alk_2030*, *No_st_alk_2040* and *No_st_alk_2050*), which represent the minimum investment level required for heat production units to meet the annual heat demand.

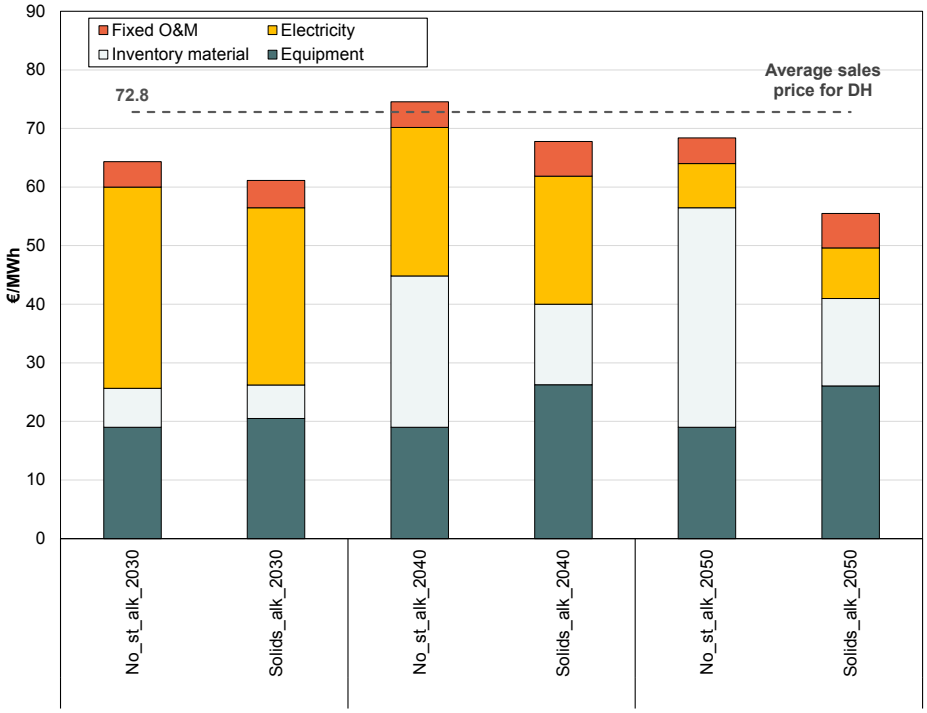

Figure 5.3: Breakdown of the heat production cost for different scenarios.

For the *Solids_alk_2030* scenario, the results show a 5 % decrease in heat production cost compared to the *No_st_alk_2030* scenario. A 9 % decrease in the heat production cost is achieved when comparing the *Solids_alk_2040* and the *No_st_alk_2040* scenarios. In the *Solids_alk_2050* scenario, this decrease in heat production cost reaches 19 % in comparison to the *No_st_alk_2050*. The lowest heat production cost is obtained in the *Solids_alk_2050* scenario, with a value of 55.5 €/MWh. These results indicate that in a VRE-dominated electricity system with significant price fluctuations, incorporating storage and heat production linked to electricity price variations can decrease the overall cost of heat production.

Despite an increase in the variability in the electricity price profiles between 2030 and 2050, the share of the electricity cost is reduced from 49.5 % in *Solids_alk_2030* to 15.6 % in *Solids_alk_2050*. This is achieved by increasing the investment both in equipment and in inventory material, from 33.5 % and 9.4% in the *Solids_alk_2030* scenario to 47 % and 26.9 % in *Solids_alk_2050*, respectively. Therefore, these results are in line with the observations presented in Section 5.1 regarding the trends in equipment and inventory material investments in response to the variability of

electricity prices.

When comparing the heat production cost of the proposed process scheme for electrifying DH plants using TCES to other solutions such as biomass-fired boilers for DH systems, several advantages can be highlighted. According to [78], combustion in bubbling fluidized bed (BFB) and circulating fluidized bed (CFB) boilers, has a Levelized Cost of Electricity (LCOE) range between 0.06 USD/kWh and 0.21 USD/kWh, depending on the availability of low-cost boilers and low-cost biomass fuels. By incorporating power generation cost data for BFB and CFB boilers, along with the assumed electrical efficiency, it is possible to estimate the heat production cost.

The study by [78] shows that the share of fuel costs in the LCOE can vary from 36% to 61% depending on the cost of the biomass fuel used in the boilers. As of 2021, biomass costs have significantly increased, with industrial wood pellets costing around €350/t and industrial wood chips costing around €160/t [79–81]. These prices are volatile and significantly affect the feasibility of constructing new biomass-fired plants.

Figure 5.4 presents the heat production cost of biomass-fired heating plants operating on BFB and CFB boilers for different biomass fuel costs. The CAPEX for both reactor types has been scaled from the data provided in [78], using a scale factor of 0.6 and assuming a capacity of 100 MW. The dashed lines represent the best and worst-case scenarios for the proposed process scheme for electrifying DH plants, which correspond to *Solids_alk_2050* and *No_st_alk_2040*, respectively. The CAPEX distribution depicted in Figure 5.2 indicates that the investment in equipment for the reduction reactor accounts for 15% of the total investment cost. To estimate the installation cost of an oxidation reactor, the cost of the reduction reactor has been doubled. This assumption is reflected in the representation of the two thresholds in Figure 5.4 (*Solids_alk_2050 Oxidation reactor* and *No_st_alk_2040 Oxidation reactor*). The results indicate that when the biomass fuel cost exceeds 225 €/t, both the CFB and BFB cases taken from [78] become more expensive than implementing TCES for electrifying the DH plant.

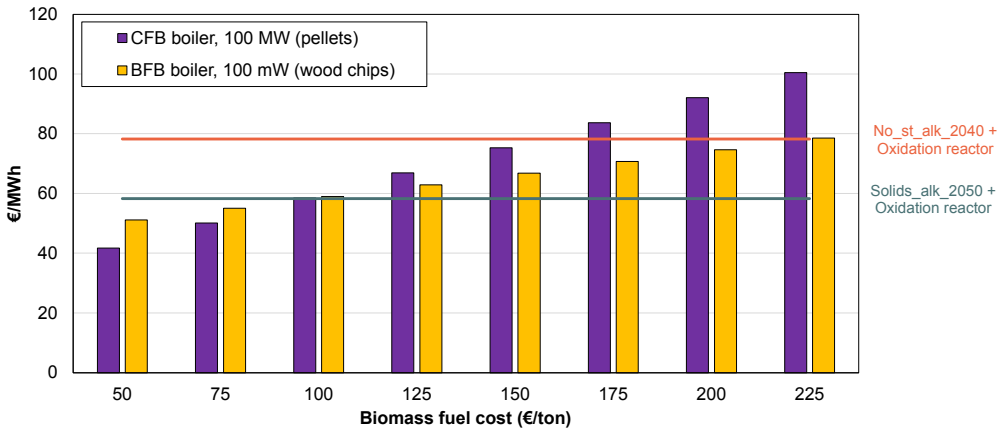

Figure 5.4: Heat production cost (y-axis) of the CFB 100 MW boiler and the BFB 100 MW boiler case when the assumed biomass fuel cost is varied (x-axis).

5.3 Sensitivity analyses

5.3.1 Inventory material cost

The share of the electricity cost out of the heat production cost is used to evaluate the sensitivity of the results to the inventory material cost for each of the electricity price profiles evaluated. The results of this analysis are depicted in Figure 4.6. When the cost of the inventory material is below 200 €/t, the model results indicate that the cost-optimal operation is running the oxidation reactor in open-loop, i.e., not investing in the charging section. Contrarily, when the cost of the inventory material exceeds 900€/t in the *Solids_alk_2050 scenario*, the cost-optimal layout involves a small (or not at all) storage capacity, i.e., it is cost-beneficial to consume more electricity than to purchase larger amounts of inventory material.

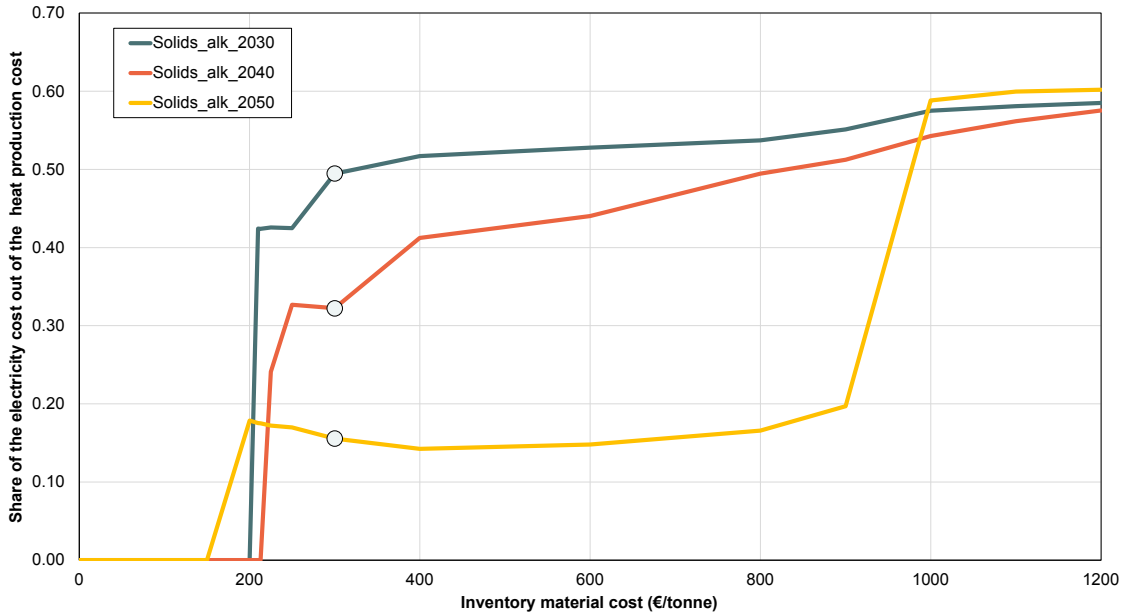

Figure 5.5: Share of the electricity cost out of the heat production cost (y-axis) for the *Solids_alk_2030*, *Solids_alk_2040* and *Solids_alk_2050* scenarios when the assumed inventory material cost is varied (x-axis). The current (2021) price of the inventory material is represented by the markers.

The results displayed in Figure 5.5 show that the variation of the inventory material costs has different impacts on the share of the electricity cost out of the heat production cost depending on the characteristics of the electricity price profile. The share of the electricity cost out of the heat production cost changes by 27 % in the *Solids_alk_2030* scenario and by 58 % in the *Solids_alk_2040* scenario when the cost of inventory material is varied from 200 to 900 €/t. However, the same increase in the cost of inventory material only results in a 14 % change in the share of the electricity cost out of the heat production cost in the *Solids_alk_2050* scenario. In this scenario, where the variability of electricity prices is the highest, the results of the modelling show that in order to provide a cost-optimal solution, investments

in inventory material must be sustained despite its increased cost. The findings highlight the significance of considering both the cost of inventory material and the electricity systems perspective when analyzing the economics of heat production with the investigated process.

5.3.2 Bare-erected cost of the high-temperature electrolyzer

The high BEC of the SOEC electrolyzer (4491 €/kWh) is a consequence of the early stage of maturity of this technology and leads to the fact that the cost-optimal size of both the charging section and storage units is zero. This means that the optimal cost solution suggests that the oxidation reactor is operated as an open-loop (constantly introducing fresh reduced iron) and the charging section is not needed (see Section 5.1). It is however foreseen that the price of the SOEC electrolyzer decreases with time, and it is, therefore, relevant to study the impact of this possible cost reduction. Figure 5.6 displays the results of the variation in the BEC of the SOEC electrolyzer in terms of the heat production cost.

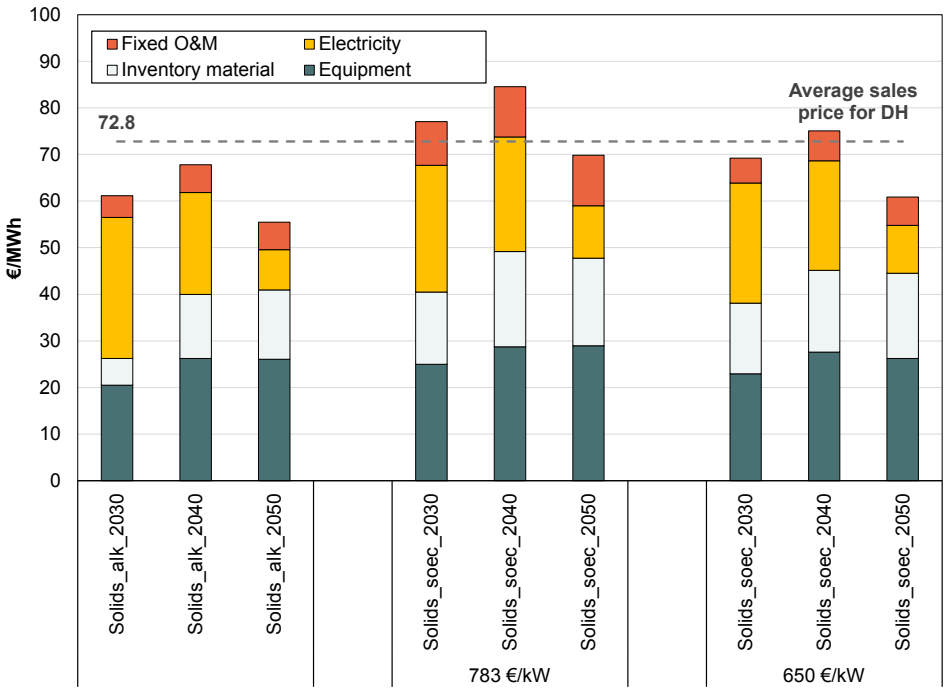

Figure 5.6: Heat production cost for the Solids_alk and Solids_soec scenarios for year 2030, 2040 and 2050. For the Solids_soec scenario, the BEC of the SOEC electrolyzer is varied according to the price reduction projections from [42].

The results of the analysis reveal that introducing SOEC technology is only economically viable if its price is reduced to the predicted BEC for 2050, according to the price reduction projections from [42]. This results in a heat production cost of 70€/MWh for the*Solids_soec_2050* scenario (BEC 783 €/kW). By further decreasing the price to match the BEC of the AEC electrolyzer in 2020 (BEC 650 €/kW),

the heat production cost is found to be 61 €/MWh, a higher cost compared to the 55 €/MWh of the *Solids_alk_2050* case (using AEC electrolyzers).

However, an important consideration when assessing the SOEC process layout is the share of energy being actually stored, which can be quantified by the dispatchability ratio as defined by Guio-Perez et al. [27]. In their study, the dispatchability ratio is introduced as a way of measuring the proportion of dispatchable heat in the total heat generated after the retrofit of the plant. The results show that the amount of dispatchable heat generated in the oxidation reactor remains constant regardless of the type of electrolyzer implemented but there is a difference in the added non-dispatchable heat production. According to [27], the dispatchability ratio is 44 % for AEC and 79 % for SOEC electrolyzer cases, due to the higher electricity consumption and higher heat losses of AEC in comparison to the SOEC electrolyzer, resulting in more non-dispatchable heat being generated. The higher the dispatchability ratio, the more flexible the operation of the plant. This flexibility has an impact on the revenues of the plant, as the selling price of dispatchable and non-dispatchable heat may vary in the future. Therefore, a cost-only model, such as the one developed and used in this thesis, falls short in accounting for the complete advantages of utilizing a SOEC electrolyzer, as it does not consider the revenue dimension.

5.4 Process economic performance

Table 5.1 summarizes the economic performance results of the plant. It can be seen that the scenarios based on the cost-optimal process layout (*Solids_alk_2030*, *Solids_alk_2040* and *Solids_alk_2050*) have a positive NPV and an IRR that exceeds the 4.75 % discount rate. This indicates that investing in the process would be profitable under the differents sets of conditions assumed in the present work. This is reinforced by the fact that the PBP for the investment is shorter than the time horizon considered in the study for all scenarios (20 years).

Table 5.1: Economic performance results for the cost-optimal process layout.

	Scenario		
	Solids_alk_2030	Solids_alk_2040	Solids_alk_2050
Net present value (NPV)	80 116 713 €	24 299 470 €	122 946 926 €
Internal rate of return (IRR)	8.7 %	5.6 %	8.6 %
Payback period (PBP)	9.4 years	11.9 years	9.4 years

The results show that the profitability of the process is highly dependent on electricity price variations and the electricity-price-following operation of the DH plant. In the *Solids_alk_2050* scenario, with the highest volatility of electricity prices, the highest return on investment is achieved, reaching an NPV of 122.9 M€. This is due to the fact that, as stated in Section 5.2, the cost savings are larger for higher electricity price volatility, which results in increased cashflows and therefore larger NPV. On the other hand, in the *Solids_alk_2040* scenario, where electricity prices

are less volatile than in 2050 but with a 33 % higher average electricity cost than in 2030, the NPV decreases to 24.3 M€, thus resulting in the lowest profitability of the three scenarios compared.

The sensitivity of the NPV to the discount rate applied is shown in Figure 5.7 for the *Solids_alk* scenario for years 2030, 2040 and 2050. The IRR can be graphically identified as the point where the function intersects the horizontal axis, i.e., where the NPV is zero. A discount rate lower than the computed IRR indicates a profitable project. According to the results displayed in Figure 5.7, the *Solids_alk_2050* scenario is more profitable than the *Solids_alk_2030* scenario when the discount rate is between 0 and 9.4 %, which is the largest IRR computed. However, if the discount rate exceeds 9.4%, the greater slope of the NPV curve for the *Solids_alk_2050* scenario would lead to greater losses compared to the *Solids_alk_2030* scenario.

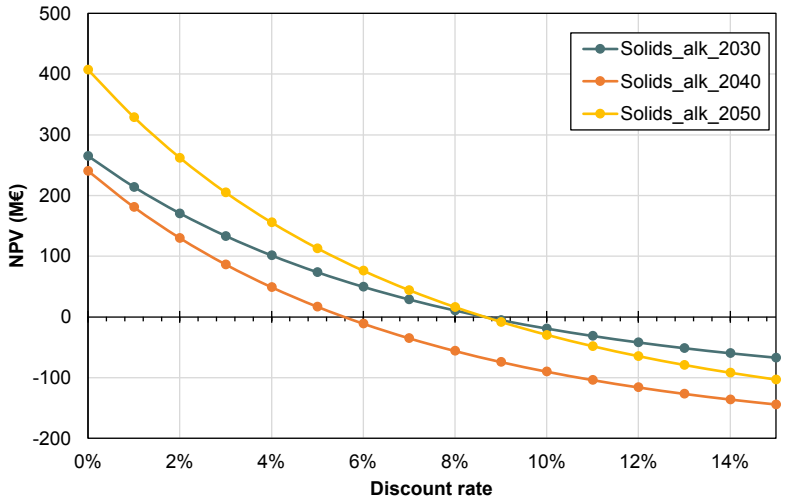

Figure 5.7: Net present value (NPV) of the electrified DH plant as a function of discount rates.

The advantages of using the proposed scheme for the electrification of DH plants are highlighted when comparing the results obtained from the economic performance analysis to that of other solutions for DH systems. One solution being considered for electrified DH systems is the use of heat pumps to recover waste heat, for example from data centres. The study conducted by Hiltunen et al. showed that in scenarios with low variability in electricity prices, an NPV of 98 M€ and a PBP of 5 years were achieved for a heat supply capacity of 100 MW [82]. When considering scenarios with higher variability in electricity, these values decreased to an NPV of 19 M€ and a PBP of 12.5 years. Another option considered for electrifying DH systems with heat pumps is to use water from rivers, lakes, or the sea as a source of low-temperature heat. The study by Pieper et al. reported that this solution could result in an NPV of 57 M€ and a PBP of 7.7 years, considering the current electricity prices [83]. These values are in line with the estimates provided by the Danish Energy Agency for the use of HP in DH systems, which typically have a PBP within the range of 4-8 years [84].

In contrast to these studies, the scheme proposed in this thesis was found to be more profitable in scenarios with larger variability in electricity prices. As explained in the work of Guío-Pérez et al., heat pumps have a dispatchability ratio of zero since they must consume electricity according to the heat demand curve, even if electricity prices are not favourable [27]. Therefore, heat pumps are not well-suited to handle the variability that characterizes systems with a large share of VRE. Contrarily, the proposed scheme introduces storage to the DH plant, resulting in a higher dispatchability of the heat supply. This dispatchability enables the operation of the DH plant to adapt and respond to variations in electricity prices. As demonstrated, this feature is highly valuable in terms of the economic viability of the scheme proposed in this thesis.

6

Conclusions

The present thesis provided an economic assessment of the retrofitting of FB-based DH plants by incorporating an iron-based redox cycle, which adds also the capacity for energy storage and the conversion of non-dispatchable into dispatchable energy. The viability of the proposed system as a practical solution for the electrification of DH plants in a VRE-dominant electricity system was studied for the Swedish case.

The cost equation of the retrofit was determined and applied as an input in a linear cost optimization model. The optimization model was set up to investigate how the variability of the electricity price impacts the cost-optimal size and operation of the units in the electrified DH plant. In addition, sensitivity analyses were conducted to assess the impact of less certain parameters (i.e., the cost of inventory material, the BEC of the SOEC electrolyzer and the discount rate) on the cost-optimal size and economic performance of the process.

The study indicates that by adapting the operation of the DH plant to respond to electricity price variations by incorporating energy storage, the cost of heat production can be reduced (approximately about 5-19 %) compared to a scenario without solids storage. The results also revealed that the electrolyzer and inventory material are the most significant cost drivers across all evaluated scenarios, while investment in hydrogen storage was found not to be an optimal addition.

The comparison of the cost of heat production between the proposed scheme for the electrification of DH plants using TCES and a combustion-based biomass scheme, shows that the process proposed in this thesis is cost-competitive with current market prices for biomass fuel. The presented process proves to be less expensive than biomass combustion at a biomass price of €225/t.

The outcome of the sensibility analyses showed that the cost of inventory material has an impact on the optimal size and operation of the plant, causing more electricity to be consumed to compensate for the rising material costs. Furthermore, the study highlights that the economic viability of using SOEC electrolyzers (as an alternative to alkaline electrolyzers) relies on the potential reduction in the bare-erected cost during the following years as the technology matures. Finally, the results of the economic performance analysis showed that the proposed process scheme is profitable for the investigated scenarios.

The Swedish case study helps to understand better the characteristics of the proposed system as a practical solution for the electrification of district heating plants in a VRE-dominant electricity system. Countries with existing metal extraction

and processing infrastructure, as well as a fleet of FB-based DH plants, could also benefit from this process.

6.1 Future work

The process scheme investigated in this thesis presents several opportunities for future work. One area of focus could be the detailed assessment of electricity production through the proposed process. The oxidation of reduced iron oxide with air in FB reactors takes place at high temperatures (up to 1100 °C), allowing for the simultaneous generation of electricity and high-temperature heat. This is especially interesting for CHP plants, which have an already-existing power production infrastructure. The potential for heat and power cogeneration also enhances the energy system's flexibility by enabling the use of DH plants to absorb electricity during low-price periods and generate electricity during high-price periods.

Another aspect that requires further investigation is the dispatchability of heat. Dispatchability is a critical component of the proposed TCES process since, the higher the dispatchability ratio, the more flexible the operation of the plant. The cost-only model developed and used in this thesis does not fully account for the advantages of utilizing high dispatchability configurations such as the one with SOEC electrolyzers, as it does not consider the revenue dimension. Thus, further research is necessary to consider the revenue dimension of heat in a profit-maximizing optimization model to explore more in detail potentially advantageous configurations.

Bibliography

[1] *Paris Agreement*. URL: https://treaties.un.org/pages/ViewDetails.aspx?src=TREATY&mtdsg_no=XXVII-7-d&chapter=27&clang=_en (visited on 09/23/2022).

[2] IEA. *Energy Statistics Data browser – data tools*. 2022. URL: https://www.iea.org/data-and-statistics/data-tools/energy-statistics-data-browser?country=UK&fuel=Energy+supply&indicator=TESbySource.

[3] International Renewable Energy Agency. "Renewable power generation costs in 2021". In: (2022). URL: www.irena.org.

[4] Lisa Göransson and Filip Johnsson. "A comparison of variation management strategies for wind power integration in different electricity system contexts". In: *Wind Energy* 21 (10 Oct. 2018), pp. 837–854. ISSN: 10991824. DOI: 10.1002/we.2198.

[5] Lisa Göransson et al. "The benefit of collaboration in the North European electricity system transition—System and sector perspectives". In: *Energies* 12 (24 Dec. 2019). ISSN: 19961073. DOI: 10.3390/en12244648.

[6] Peter D. Lund et al. "Review of energy system flexibility measures to enable high levels of variable renewable electricity". In: *Renewable and Sustainable Energy Reviews* 45.C (2015), pp. 785–807. URL: https://EconPapers.repec.org/RePEc:eee:rensus:v:45:y:2015:i:c:p:785-807.

[7] European Parliament and Council. *Amending Directive (EU) 2018/2001 of the European Parliament and of the Council, Regulation (EU) 2018/1999 of the European Parliament and of the Council and Directive 98/70/EC of the European Parliament and of the Council as regards the promotion of energy from renewable sources, and repealing Council Directive (EU) 2015/652*. https://eur-lex.europa.eu/legal-content/EN/TXT/?uri=CELEX:52021PC05579. 2021.

[8] E. J. Anthony. "Fluidized bed combustion of alternative solid fuels; status, successes and problems of the technology". In: *Progress in Energy and Combustion Science* 21 (3 Jan. 1995), pp. 239–268. ISSN: 0360-1285. DOI: 10.1016/0360-1285(95)00005-3.

[9] Guillermo Martínez Castilla et al. "Techno-economic assessment of calcium looping for thermochemical energy storage with CO_2 capture". In: *Energies* 14 (11 June 2021). ISSN: 19961073. DOI: 10.3390/en14113211.

[10] Huashan Bao and Zhiwei Ma. "28 - Thermochemical energy storage". In: ed. by Trevor M Letcher. Second Edition. Elsevier, 2022, pp. 651–683. ISBN: 978-0-12-824510-1. DOI: https://doi.org/10.1016/B978-0-12-824510-

1.00028-3. URL: https://www.sciencedirect.com/science/article/pii/B9780128245101000283.

[11] Jeffrey M. Bergthorson. "Recyclable metal fuels for clean and compact zero-carbon power". In: *Progress in Energy and Combustion Science* 68 (Sept. 2018), pp. 169–196. ISSN: 03601285. DOI: 10.1016/j.pecs.2018.05.001.

[12] Sike Wu et al. "A review on high-temperature thermochemical energy storage based on metal oxides redox cycle". In: *Energy Conversion and Management* 168 (July 2018), pp. 421–453. ISSN: 0196-8904. DOI: 10.1016/J.ENCONMAN.2018.05.017.

[13] Pierre Pardo et al. "Review on high temperature thermochemical heat energy storage". In: *Renewable and Sustainable Energy Reviews* 32 (Apr. 2014), pp. 591–610. DOI: 10.1016/j.rser.2013.12.014.

[14] J. Sunku Prasad et al. "A critical review of high-temperature reversible thermochemical energy storage systems". In: *Applied Energy* 254 (Nov. 2019), p. 113733. ISSN: 0306-2619. DOI: 10.1016/J.APENERGY.2019.113733.

[15] Carlos Ortiz et al. "Scaling-up the Calcium-Looping Process for CO_2 Capture and Energy Storage". In: *KONA Powder and Particle Journal* 38 (Jan. 2021), pp. 189–208. ISSN: 0288-4534. DOI: 10.14356/KONA.2021005.

[16] Yongliang Yan et al. "Developments in calcium/chemical looping and metal oxide redox cycles for high-temperature thermochemical energy storage: A review". In: *Fuel Processing Technology* 199 (Mar. 2020), p. 106280. ISSN: 0378-3820. DOI: 10.1016/J.FUPROC.2019.106280.

[17] Stylianos Flegkas et al. "Profitability Analysis and Capital Cost Estimation of a Thermochemical Energy Storage System Utilizing Fluidized Bed Reactors and the Reaction System MgO/Mg(OH)2". In: *Energies 2019, Vol. 12, Page 4788* 12 (24 Dec. 2019), p. 4788. ISSN: 1996-1073. DOI: 10.3390/EN12244788. URL: https://www.mdpi.com/1996-1073/12/24/4788/htm%20https://www.mdpi.com/1996-1073/12/24/4788.

[18] E. Mastronardo et al. "Efficiency improvement of heat storage materials for MgO/H2O/Mg(OH)2 chemical heat pumps". In: *Applied Energy* 162.C (2016), pp. 31–39. DOI: 10.1016/j.apenergy.2015.1. URL: https://ideas.repec.org/a/eee/appene/v162y2016icp31-39.html.

[19] Matthias Schmidt, Marie Gollsch, and Franz Giger. "Development of a moving bed pilot plant for thermochemical energy storage with CaO/ Ca(OH)2". In: 1734 (2016), p. 50041. DOI: 10.1063/1.4949139. URL: https://doi.org/10.1063/1.4949139.

[20] Laurie André and Stéphane Abanades. "Recent Advances in Thermochemical Energy Storage via Solid–Gas Reversible Reactions at High Temperature". In: *Energies 2020, Vol. 13, Page 5859* 13 (22 Nov. 2020), p. 5859. ISSN: 1996-1073. DOI: 10.3390/EN13225859. URL: https://www.mdpi.com/1996-1073/13/22/5859/htm%20https://www.mdpi.com/1996-1073/13/22/5859.

[21] Laurie André, Stéphane Abanades, and Laurent Cassayre. "High-temperature thermochemical energy storage based on redox reactions using Co-Fe and Mn-Fe mixed metal oxides". In: *Journal of Solid State Chemistry* 253 (Sept. 2017), pp. 6–14. ISSN: 0022-4596. DOI: 10.1016/J.JSSC.2017.05.015.

[22] Tina Block and Martin Schmücker. "Metal oxides for thermochemical energy storage: A comparison of several metal oxide systems". In: *Solar Energy* 126 (Mar. 2016), pp. 195–207. ISSN: 0038092X. DOI: 10.1016/J.SOLENER.2015.12.032.

[23] Alfonso J. Carrillo et al. "Thermochemical energy storage at high temperature via redox cycles of Mn and Co oxides: Pure oxides versus mixed ones". In: *Solar Energy Materials and Solar Cells* 123 (Apr. 2014), pp. 47–57. ISSN: 0927-0248. DOI: 10.1016/J.SOLMAT.2013.12.018.

[24] Jannik Neumann et al. "Energy and Exergy Assessment of Renewable Energy Storage using Iron as Energy Carrier". In: *SIMULATION AND ENVIRONMENTAL IMPACT OF ENERGY SYSTEMS* (2022).

[25] J. M. Bergthorson et al. "Direct combustion of recyclable metal fuels for zero-carbon heat and power". In: *Applied Energy* 160 (Dec. 2015), pp. 368–382. ISSN: 03062619. DOI: 10.1016/J.APENERGY.2015.09.037.

[26] P. Debiagi et al. "Iron as a sustainable chemical carrier of renewable energy: Analysis of opportunities and challenges for retrofitting coal-fired power plants". In: *Renewable and Sustainable Energy Reviews* 165 (Sept. 2022). ISSN: 18790690. DOI: 10.1016/j.rser.2022.112579.

[27] Diana Carolina Guío-Pérez et al. "Thermochemical Energy Storage with Integrated District Heat Production-A Case Study of Sweden". In: 16 (2023), p. 1155. DOI: 10.3390/en16031155.

[28] Swedish Energy Agency. *Energy in Sweden 2022 – An overview*. Swedish Energy Agency, Sept. 2022.

[29] IEA-FBC TCP. *Developments in fluidized bed conversion during 2011-2016*. IEA, Dec. 2017, pp. 102–105.

[30] Göteborg Energi AB. *Environmental report 2021 - Rya Hetvattencentral and Gobigas*. Göteborg Energi, 2021.

[31] Valmet. *Valmet to supply a hot water plant to Göteborg Energi in Sweden*. June 2020. URL: https://www.valmet.com/media/news/press-releases/2020/valmet-to-supply-a-hot-water-plant-to-goteborg-energi-in-sweden/.

[32] Göteborg Energi AB. *Environmental report 2021 - Sävenäsverket*. Göteborg Energi, 2021.

[33] Geological Survey of Sweden. *Bergverksstatistik 2019. Statistics of the Swedish mining industry*. Geological Survey of Sweden, 2020. URL: https://www.sgu.se/en/mineral-resources/mineral-statistics/ore-production-and-trends/.

[34] Geological Survey of Sweden. *Swedish mines*. 2020. URL: https://www.sgu.se/en/mineral-resources/swedish-mines/ (visited on 12/08/2022).

[35] *The Swedish Steel Industry*. URL: https://www.jernkontoret.se/en/the-steel-industry/.

[36] LKAB, SSAB, and Vattenfall. *Fossil-free Steel - Hybrit*. URL: https://www.hybritdevelopment.se/en/ (visited on 01/23/2023).

[37] Johannes Leopold Schenk. "Recent status of fluidized bed technologies for producing iron input materials for steelmaking". In: *Particuology* 9 (1 Feb. 2011), pp. 14–23. ISSN: 16742001. DOI: 10.1016/J.PARTIC.2010.08.011.

[38] Daizo Kunii and Octave Levenspiel. "CHAPTER 6 - Bubbling Fluidized Beds". In: *Fluidization Engineering (Second Edition)*. Ed. by Daizo Kunii and Octave Levenspiel. Second Edition. Boston: Butterworth-Heinemann, 1991, pp. 137–164. ISBN: 978-0-08-050664-7. DOI: https://doi.org/10.1016/B978-0-08-050664-7.50012-3. URL: https://www.sciencedirect.com/science/article/pii/B9780080506647500123.

[39] Metso Outotec. *Fine Ore Direct Reduction - Circored*. Metso Outotec, 2021.

[40] S.A. Elmquist, P. Weber, and H. Eichberger. "Operational results of the Circored fine ore direct reduction plant in Trinidad". In: *Stahl und Eisen* 122 (Feb. 2002), pp. 59–64.

[41] Blue Spark Admin User. *Hot briquetted iron (HBI)*. Nov. 2017. URL: https://www.metallics.org/hbi.html.

[42] Danish Energy Agency. *Technology Data for Renewable Fuels*. 2017, pp. 94–118. URL: http://www.ens.dk/teknologikatalog.

[43] Haoran Li and Natasa Nord. "Transition to the 4th generation district heating - possibilities, bottlenecks, and challenges". In: *Energy Procedia* 149 (Sept. 2018), pp. 483–498. DOI: 10.1016/j.egypro.2018.08.213.

[44] Sven Werner. "District heating and cooling in Sweden". In: *Energy* 126 (2017), pp. 419–429. ISSN: 03605442. DOI: 10.1016/j.energy.2017.03.052.

[45] I Dincer and C Zamfirescu. "Hydrogen production by electrical energy". In: *Sustainable Hydrogen Production* (2016), pp. 99–161.

[46] IEA. *Hydrogen Supply*. IEA, 2022. URL: https://www.iea.org/reports/hydrogen-supply.

[47] International Energy Agency - IEA. *Global Hydrogen Review 2022*. 2022. URL: www.iea.org/t&c/.

[48] Oliver Schmidt et al. "Future cost and performance of water electrolysis: An expert elicitation study". In: *International Journal of Hydrogen Energy* 42 (52 Dec. 2017), pp. 30470–30492. ISSN: 03603199. DOI: 10.1016/J.IJHYDENE.2017.10.045.

[49] Kai Zeng and Dongke Zhang. "Recent progress in alkaline water electrolysis for hydrogen production and applications". In: *Progress in energy and combustion science* 36.3 (2010), pp. 307–326.

[50] Fredrik Jonsson and Andrea Miljanovic. "Utilization of waste heat from hydrogen production". Mälardalen University, June 2022. URL: https://www.diva-portal.org/smash/get/diva2:1670187/FULLTEXT01.pdf.

[51] Saman Rashidi et al. "Progress and challenges on the thermal management of electrochemical energy conversion and storage technologies: Fuel cells, electrolysers, and supercapacitors". In: *Progress in Energy and Combustion Science* 88 (2022), p. 100966. ISSN: 0360-1285. DOI: https://doi.org/10.1016/j.pecs.2021.100966. URL: https://www.sciencedirect.com/science/article/pii/S0360128521000642.

[52] Kai Zeng and Dongke Zhang. "Recent progress in alkaline water electrolysis for hydrogen production and applications". In: *Progress in Energy and Combustion Science* 36.3 (2010), pp. 307–326. ISSN: 0360-1285. DOI: https://doi.org/10.1016/j.pecs.2009.11.002. URL: https://www.sciencedirect.com/science/article/pii/S0360128509000598.

[53] Joachim Werther. "Fluidized-Bed Reactors". In: *Ullmann's Encyclopedia of Industrial Chemistry*. John Wiley Sons, Ltd, 2007. ISBN: 9783527306732. DOI: https://doi.org/10.1002/14356007.b04_239.pub2. eprint: https://onlinelibrary.wiley.com/doi/pdf/10.1002/14356007.b04_239.pub2. URL: https://onlinelibrary.wiley.com/doi/abs/10.1002/14356007.b04_239.pub2.

[54] Dimitri Mignard and Colin Pritchard. "A review of the sponge iron process for the storage and transmission of remotely generated marine energy". In: *International Journal of Hydrogen Energy* 32 (18 Dec. 2007), pp. 5039–5049. ISSN: 03603199. DOI: 10.1016/j.ijhydene.2007.06.032.

[55] Daniel Spreitzer and Johannes Schenk. "Iron Ore Reduction by Hydrogen Using a Laboratory Scale Fluidized Bed Reactor: Kinetic Investigation—Experimental Setup and Method for Determination". In: *Metallurgical and Materials Transactions B: Process Metallurgy and Materials Processing Science* 50 (5 Oct. 2019), pp. 2471–2484. ISSN: 10735615. DOI: 10.1007/S11663-019-01650-9/FIGURES/15. URL: https://link.springer.com/article/10.1007/s11663-019-01650-9.

[56] International Council on Mining Metals. *Hazard Assessment of Ores and Concentrates for Marine Transport*. ICMM, Apr. 2021.

[57] International Iron Metallics Association. *Direct Reduced Iron (DRI): Guide to Shipping, Handling and Storage*. IIMA, Apr. 2022.

[58] Ilias Vorrias et al. "Calcium looping for CO_2 capture from a lignite fired power plant". In: *Fuel* 113 (Nov. 2013), pp. 826–836. ISSN: 0016-2361. DOI: 10.1016/J.FUEL.2012.12.087.

[59] Radoslaw Tarkowski. "Underground hydrogen storage: Characteristics and prospects". In: *Renewable and Sustainable Energy Reviews* 105 (2019), pp. 86–94. ISSN: 1364-0321. DOI: https://doi.org/10.1016/j.rser.2019.01.051. URL: https://www.sciencedirect.com/science/article/pii/S1364032119300528.

[60] Danish Energy Agency. *Technology Data - Energy storage*. 2018. URL: http://www.ens.dk/teknologikatalog.

[61] Sune Ebbesen et al. "High Temperature Electrolysis in Alkaline Cells, Solid Proton Conducting Cells, and Solid Oxide Cells". In: *Chemical reviews* 114 (Oct. 2014). DOI: 10.1021/cr5000865.

[62] John Bøgild Hansen. "Solid oxide electrolysis – a key enabling technology for sustainable energy scenarios". In: *Faraday Discussions* 182 (0 Nov. 2015), pp. 9–48. ISSN: 1364-5498. DOI: 10.1039/C5FD90071A. URL: https://pubs.rsc.org/en/content/articlehtml/2015/fd/c5fd90071a%20https://pubs.rsc.org/en/content/articlelanding/2015/fd/c5fd90071a.

[63] Giampaolo Manzolini, Ennio Macchi, and Matteo Gazzani. "CO_2 capture in Integrated Gasification Combined Cycle with SEWGS – Part B: Economic assessment". In: *Fuel* 105 (2013), pp. 220–227. ISSN: 0016-2361. DOI: https://doi.org/10.1016/j.fuel.2012.07.043. URL: https://www.sciencedirect.com/science/article/pii/S0016236112005923.

[64] Larry R. Dysert. "So You Think You're an Estimator?" In: *Cost engineering* 47 (2005), pp. 30–35.

[65] G. Towler and R. Sinnott. *Chemical Engineering Design (Third Edition)*. Butterworth-Heinemann, 2022. ISBN: 9780128211793. URL: https://www.sciencedirect.com/science/article/pii/B9780128211793150010.

[66] R. Turton et al. *Analysis, Synthesis and Design of Chemical Processes*. Prentice Hall International Series in the Physical and Chemical Engineering Sciences. Pearson Education, 2008. ISBN: 9780132459181. URL: https://books.google.se/books?id=kWXyhVXztZ8C.

[67] D. R. Woods. *Rules of Thumb in Engineering Practice*. John Wiley Sons, Ltd, 2007. ISBN: 9783527611119. URL: https://onlinelibrary.wiley.com/doi/abs/10.1002/9783527611119.app4.

[68] Henrik Thunman and Martin Seemann. "The gobigas plant". In: Elsevier, Jan. 2019, pp. 455–474. ISBN: 9780128155547. DOI: 10.1016/B978-0-12-815554-7.00017-9.

[69] Danish Energy Agency. *Technology Data - Energy Plants for Electricity and District heating generation*. 2017. URL: http://www.ens.dk/teknologikatalog.

[70] Henrik Thunman et al. "Economic assessment of advanced biofuel production via gasification using cost data from the GoBiGas plant". In: *Energy Science Engineering* 7 (1 Feb. 2019), pp. 217–229. ISSN: 2050-0505. DOI: 10.1002/ESE3.271. URL: https://onlinelibrary.wiley.com/doi/full/10.1002/ese3.271%20https://onlinelibrary.wiley.com/doi/abs/10.1002/ese3.271%20https://onlinelibrary.wiley.com/doi/10.1002/ese3.271.

[71] Sebastian Michalski, Dawid P. Hanak, and Vasilije Manovic. "Techno-economic feasibility assessment of calcium looping combustion using commercial technology appraisal tools". In: *Journal of Cleaner Production* 219 (May 2019), pp. 540–551. ISSN: 0959-6526. DOI: 10.1016/J.JCLEPRO.2019.02.049.

[72] Alicia Bayon et al. "Techno-economic assessment of solid–gas thermochemical energy storage systems for solar thermal power applications". In: *Energy* 149 (Apr. 2018), pp. 473–484. ISSN: 0360-5442. DOI: 10.1016/J.ENERGY.2017.11.084.

[73] Alla Toktarova, Lisa Göransson, and Filip Johnsson. "Design of clean steel production with hydrogen: Impact of electricity system composition". In: (2021). DOI: 10.3390/en14248349. URL: http://dx.doi.org/10.3390/en14248349.

[74] M. Åberg, L. Fälting, and A. Forssell. "Is Swedish district heating operating on an integrated market? - Differences in pricing, price convergence, and marketing strategy between public and private district heating companies". In: *Energy Policy* 90 (Mar. 2016), pp. 222–232. ISSN: 03014215. DOI: 10.1016/j.enpol.2015.12.030.

[75] European Commission, Directorate-General for Regional, and Urban Policy. *Guide to cost-benefit analysis of investment projects : economic appraisal tool for cohesion policy 2014-2020*. Publications Office, 2015. DOI: doi/10.2769/97516.

[76] Market Reports World. *Hot Briquetted Iron (HBI) Market Size, Share, Growth | Analysis Report, 2022-2028*. Apr. 2022. URL: https://www.yahoo.com/entertainment/hot-briquetted-iron-hbi-market-123900809.html.

[77] Roberto Somorra. *Brazil miner Vale considers making low-emission iron if gas prices fall: sources*. Oct. 2019. URL: https://www.reuters.com/article/

us-vale-sa-products/brazil-miner-vale-considers-making-low-emission-iron-if-gas-prices-fall-sources-idUSKBN1WJ061.

[78] International Renewable Energy Agency. *Renewable Energy Technologies Cost Analysis Series: Biomass Power Generation*. Technical report. International Renewable Energy Agency, 2012. URL: https://www.irena.org/-/media/Files/IRENA/Agency/Publication/2012/RE_Technologies_Cost_Analysis-BIOMASS.pdf.

[79] Argus Media. *Biomass Markets*. https://www.argusmedia.com/-/media/Files/sample-reports/argus-biomass-markets.ashx?la=en&hash=872E2C03A0A78FE3F236BBF00E7729E3114326E0. Accessed on: March 13, 2023. Jan. 2023.

[80] Baltic Energy Exchange. *Biomass Trade Statistics: February of 2023*. https://www.baltpool.eu/en/biomass-trade-statistics-february-of-2023/. Accessed on: March 13, 2023. 2023.

[81] Svebio. *Nyheter om flis- och pelletsmarknaden*. https://www.svebio.se/baltpool-2/nyheter-om-flis-och-pelletsmarknaden/. Accessed on: March 13, 2023. Jan. 2022.

[82] Pauli Hiltunen and Sanna Syri. "Highly Renewable District Heat for Espoo Utilizing Waste Heat Sources". In: *Energies 2020, Vol. 13, Page 3551* 13 (14 July 2020), p. 3551. ISSN: 1996-1073. DOI: 10.3390/EN13143551. URL: https://www.mdpi.com/1996-1073/13/14/3551/htm%20https://www.mdpi.com/1996-1073/13/14/3551.

[83] Henrik Pieper et al. "Modelling framework for integration of large-scale heat pumps in district heating using low-temperature heat sources: A case study of Tallinn, Estonia". In: *International Journal of Sustainable Energy Planning and Management* 20 (2019), pp. 67–86. ISSN: 22462929. DOI: 10.5278/ijsepm.2019.20.6.

[84] Hanne Kortegaard Støchkel, Bjarke Lava Paaske, and Kim Clausen. *Inspirationskatalog for store varmepumpeprojekter i fjernvarmesystemet*. Grøn Energi, PlanEnergi, DFP, Dec. 2017.

[85] "Heat pump COP, part 2: Generalized COP estimation of heat pump processes". In: vol. 2018-June. International Institute of Refrigeration, 2018, pp. 1255–1264. ISBN: 9782362150265. DOI: 10.18462/iir.gl.2018.1386.

[86] Mateo Jesper et al. "Large-scale heat pumps: Uptake and performance modelling of market-available devices". In: *Renewable and Sustainable Energy Reviews* 137 (Mar. 2021). ISSN: 18790690. DOI: 10.1016/J.RSER.2020.110646.

[87] Anton Larsson, Ingemar Gunnasrsson, and Freddy Tengberg. *The GoBiGas Project Demonstration of the Production of Biomethane from Biomass via Gasification*. 2018.

A

Appendix A

A.1 Sizing of the units

A.1.1 Alkaline electrolyzer waste heat recovery

The COP is a measure of the efficiency of a HP. When calculating the COP of a HP, the heat output of the condenser is compared to the power supplied to the compressor, thus the ratio between the heat yielded by the system and the power supplied by the compressor often takes higher values to the unit. Modelling the thermodynamic cycle of the HP can be a laborious task that requires an optimization process, which escapes the scope of the present thesis. Therefore, it has been chosen to assume a constant COP, which will be calculated throughout this section.

The theoretical limit for the COP of a HP operating between a hot and cold focus with constant temperatures is defined by the Carnot COP (COP_{Car}). The Lorenz COP (COP_{Lor}) is an expression based on the mean temperature differences of the source and the sink to calculate the coefficient of performance of an infinite number of HP processes. On the one hand, the Lorenz efficiency can be defined as the ratio between the actual COP of the HP and Lorenz COP (Equation A.1)

$$\eta_{Lor} = \frac{COP}{COP_{Lor}} \tag{A.1}$$

On the other hand, η_{2nd} compares the real COP of a HP and the Carnot COP (see Equation A.2).

$$\eta_{2nd} = \frac{COP}{COP_{Car}} \tag{A.2}$$

The methodology proposed by Jensen et al. in [85] has been used for calculating the actual COP of a HP using the parameters presented in A.1:

Table A.1: Parameters used for the COP characterization of the HP.

Parameter	Value
$T_{hot,out}$	90 °C
$T_{hot,in}$	40 °C
$T_{cold,out}$	75 °C
$T_{cold,in}$	80 °C
c_p (77.5 °C)	4.194 $\frac{KJ}{k \cdot kg}$

The results obtained are depicted in Table A.2. A value of 6.142 was obtained for the COP of the HP. According to Jensen et al., the typical value for the η_{Lor} is 0.25 for HP operating with temperature lifts within 10-15 °C [85], while for the η_{2nd} values around 0.25 are provided by Jesper et al. for HP operating under similar conditions [86]. Thus, the results obtained from the sizing of the unit are validated and a value of 6.142 is used as the actual COP of the HP.

Table A.2: Results from the COP characterization of the HP.

Variable	Value
COP	6.142
COP_{Carnot}	24.21
COP_{Lorenz}	25.74
η_{2nd}	0.25
η_{Lor}	0.24

A.1.2 Reduction reactor

The method presented by Flegkas et al. has been used to determine the volume of the reactor $V_{reactor}$ [17]. The product of particle residence time τ_p and the reducing solid material stream $\dot{m}_s$ yields the particle mass M_{TCM} inside the reactor:

$$M_{TCM} = \tau_p \cdot \dot{m}_s \tag{A.3}$$

The bed volume V_{bed} can be obtained through the particle bulk density ρ_{bulk}:

$$V_{bed} = \frac{M_{TCM}}{\rho_{bulk}} \tag{A.4}$$

The freeboard over the bed is assumed to be three times the volume of the bed. Finally, the total volume of the reactor is given by

$$V_{reactor} = 3 \cdot V_{bed} \tag{A.5}$$

The parameters used for evaluating the equations are:

Table A.3: Parameters used for preliminary sizing of the reduction reactor.

Parameter	Value
τ_p	100 min
ρ_{bulk}	2500 kg/m3

Regarding the heat recovery of the steam of the reduction reactor, the following parameters are used for the preliminary sizing of the cooler and the condenser.

Table A.4: Parameters used for preliminary sizing of the desuperheater and the condenser for the recovery of waste heat from the steam outlet of the reactor in the main process design.

DH2 - Desuperheater	
Steam parameter	Value
T_{in}	1100 °C
P_{in}	1 bar
h_{in}	4893.5
T_{out}	99.63 °C
P_{out}	1 bar
h_{out}	2675.5 kJ/kg
DH Water parameter	Value
T_{in}	40 °C
T_{out}	90 °C
Heat exchanger parameter	Value
U	1500 W/m2K

DH2 - Condenser	
Steam-Water parameter	Value
T_{in}	99.63 °C
P_{in}	1 bar
h_{in}	2675.5 kJ/kg
T_{out}	99.63 °C
T_{out}	1 bar
h_{out}	417.46 kJ/kg
DH Water parameter	Value
T_{in}	40 °C
T_{out}	90 °C
Heat exchanger parameter	Value
U	1500 W/m2K

A.1.3 Solids storage

The design of a storage tank from Bayon et al. has been used as a design basis for the solids storage units for the proposed process [72]. The parameters used for the calculations are shown in Table A.5.

Table A.5: Selected parameters for the calculation of the total mass of steel for both the reduced and the oxidized material storage.

Parameter	**Value**
Price of steel	698.40 €/t
Density of steel	7874 kg/m3
Brick height	0.0572 m
Brick wide	0.0921 m
Brick lenght	0.2032 m

A.2 The GoBiGas project

The Gothenburg Biomass Gasification (GoBiGas) plant, which began its operation in the spring of 2005, used gasification on an industrial scale to convert biomass into advanced biofuel [68]. The plant operated for more than 12000 hours and was able to produce high-quality gas from biomass gasification using various feedstocks like bark, wood pellets, or chips. Due to unfavorable market conditions, the plant could not transition from demonstration to commercial level and was mothballed in 2018.

Figure A.1 presents the schematic of the GoBiGas plant. The production process was divided into two steps. The first was the dual fluidized bed (DFB) gasification step; converting biomass to gas. In the second step, the gas was converted to specific hydrocarbon(s), methane in the case of the GoBiGas plant.

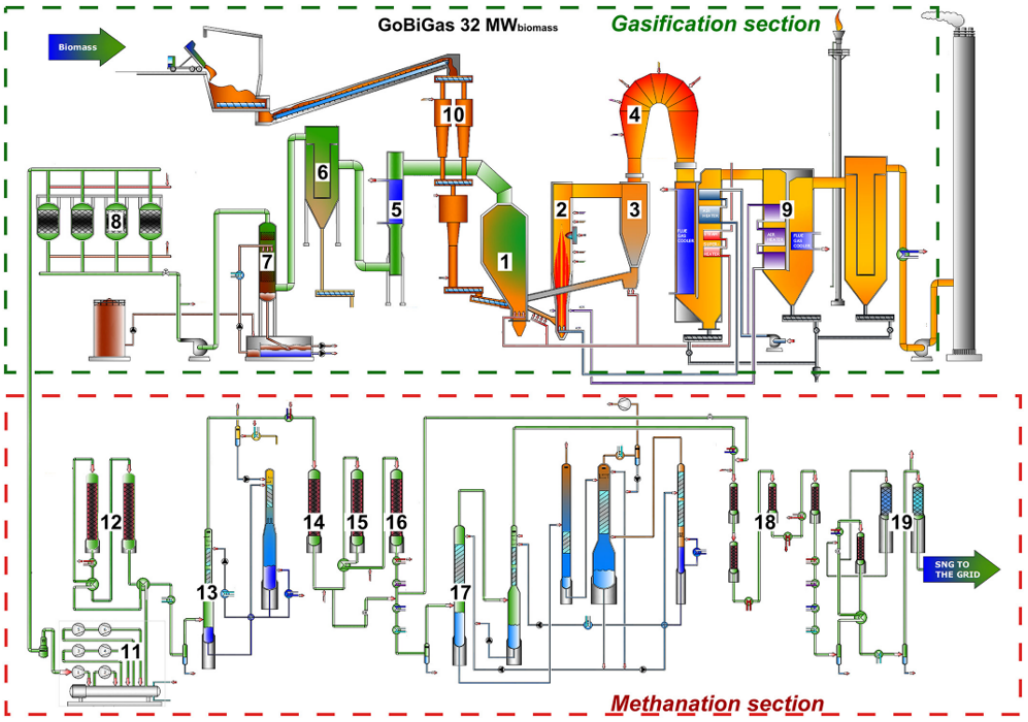

Figure A.1: Schematic overview of the GoBiGas-plant: 1, gasifier; 2, combustion chamber; 3, cyclone; 4, post-combustion chamber; 5, raw gas cooler; 6, raw gas filter; 7, rapeseed methyl ester scrubber; 8, carbon beds; 9, flue gas train; 10, fuel feeding system; 11, product gas compressor; 12, hydration of olefins and COS; 13, H2S removal; 14, guard bed; 15, water–gas shift reactor; 16, pre-methanation; 17, CO2 removal, 18, methanation; and 19, drying. Extracted from [87]

The DFB comprised a bubbling FB gasifier and a circulating FB combustor. The reduction reactor, the focus of the present thesis, closely resembles a conventional FB gasifier. Therefore, the cost estimation can be based on the cost of the FB gasifier from GoBiGas. However, the challenge lies in the fact that DFB units are typically manufactured as an integrated system, thus the available economic data for the DFB system deployed by GoBiGas only reflects the overall cost of the equipment,

without differentiating between the costs incurred by the gasifier and the combustor components [70].

A sensitivity analysis was performed on the BEC of the reduction reactor composing the proposed schemes when varying the reference cost used in Equarion 4.1 (see Figure A.2). The reference cost is varied between different shares of the gasifier cost over the total cost of the DFB from the GoBiGas plant.

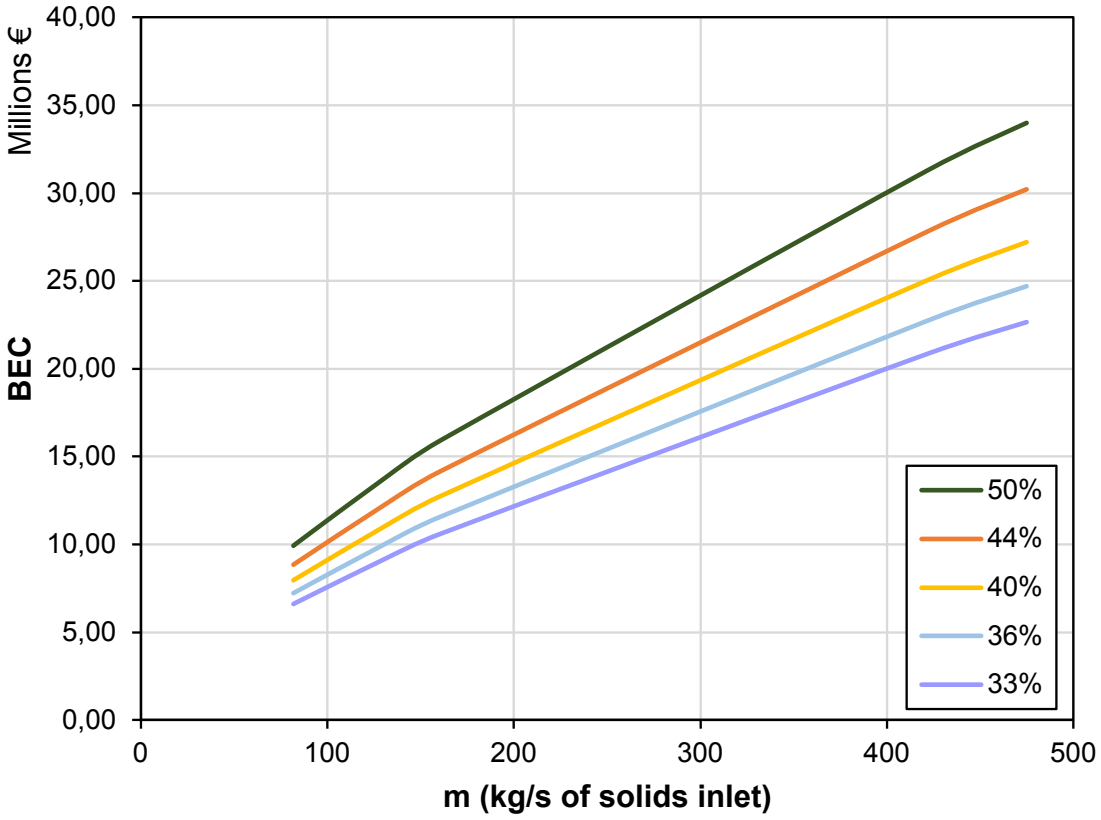

Figure A.2: BEC of the reduction reactor composing the proposed schemes when varying the reference cost used in the cost equation. The cost is varied between different shares of the gasifier cost over the total cost of the DFB from the GoBiGas plant.

It is chosen to assume that the weight of the gasifier is 40% of the total reference cost. Thus, equation 4.2 shows the final expression used for calculating the cost of equipment of the reduction reactor.

DEPARTMENT OF SPACE, EARTH AND ENVIRONMENT
CHALMERS UNIVERSITY OF TECHNOLOGY
Gothenburg, Sweden
www.chalmers.se

CHALMERS
UNIVERSITY OF TECHNOLOGY